Fall 12-2013

Adsorption/Desorption Process of Stimuli-Responsive Polymers on Simulated Natural Surfaces Using QCM-D & AFM Analysis

Yan Zong
University of Southern Mississippi

The University of Southern Mississippi

ADSORPTION/DESORPTION PROCESS OF STIMULI-RESPONSIVE POLYMERS ON SIMULATED NATURAL SURFACES USING QCM-D & AFM ANALYSIS

by

Yan Zong

A Thesis
Submitted to the Graduate School
of The University of Southern Mississippi
in Partial Fulfillment of the Requirements
for the Degree of Master of Science

Approved:

Dean of the Graduate School

December 2013

ABSTRACT

ADSORPTION/DESORPTION PROCESS OF STIMULI-RESPONSIVE POLYMERS ON SIMULATED NATURAL SURFACES USING QCM-D & AFM ANALYSIS

by Yan Zong

December 2013

The stimuli-responsive adsorption of polyelectrolytes to biosurfaces provides an important vehicle for development of protective coatings, delivery of therapeutic agents, and cosmetic applications. Developing a fundamental understanding of the mechanisms and kinetics of adsorption/desorption processes of polymeric systems to biological surfaces is of critical importance in predicting performance and designing new formulations. This study describes quartz crystal microbalance and atomic force microscopy analysis of a poly(methyl vinyl ether-alt-maleic anhydride) copolymer (Gantrez® S97 BF) adsorption on dental mimicking surfaces to determine properties including thickness, morphology, viscoelasticy, and rate of adsorption/desorption of the polymer layer as a function of solution environment. A nanoscopically smooth model dental surface was developed for AFM analysis of the adsorbed thin film. Polymer structural and solution factors controlling kinetics of adsorption and the adhesion properties on simulated hydroxyapatite (HAp) surfaces are elucidated.

The second part of the thesis focuses on the evaluation of a novel oil spill dispersant with anti-deposition capabilities. The dispersing agent is largely comprised of hydroxypropyl cellulose and lecithin, agriculturally derived chemicals commonly used in the food industry. Spilled or leaked oil is a continued threat to the environment and wildlife. Though dispersants are commonly used to combat oil spillsin the hope of using them to mitigate the effects of oil on land and wildlife, the challenge of preventing redeposition of the oil onto these substrates still exists, and there are concerns with the biocompatibility of current commercial dispersant formulations. Quartz crystal microbalance with dissipation monitoring (QCM-D) was employed to investigate the interactions of the polymer dispersants on model natural surfaces. AFM was used to investigate the morphology of films after deposition on the model surfaces. Mechanisms and kinetics of the adsorption and desorption processes of the anti-redeposition polymer formulation are described.

ACKNOWLEDGMENTS

First, I would like to give my greatest appreciation to my graduate advisor, Dr. Sarah E. Morgan, for her guidance, support and patience. Her constant direction and encouragement helped me a lot in both academic progress and personal development. Additionally, I would like to thank my other graduate committee members, Drs. Robert Y. Lochhead and Daniel A. Savin. I would also like to thank current and past members in the Morgan research group for their support and valuable friendship. I would like to give special acknowledgment to Yuhong Wei and Dr. Dipti Singh for their great help and contribution at the beginning stage of my graduate research. I had a wonderful and impressive experience during my summer internship at Johnson & Johnson Consumer & Personal Products Department in 2012. I am grateful to my two supervisors, Drs. Frank C. Sun and Michael J. Fevola, for the helpful discussion and introduction to my research. I would also like to thank Mrs. Kim Wingo for her kindness and assistance for our research group.

My primary graduate project was supported by the Partnership for Innovation (PFI) program of the National Science Foundation (NSF) under award number IIP-0917730. It was also supported through the Accelerating Innovative Research (AIR) project 1047662 awarded by the National Science Foundation (NSF).

Finally, I would to finish this acknowledgement with my gratitude to my friends and family.

TABLE OF CONTENTS

ABSTRACT ii

ACKNOWLEDGMENTS iv

LIST OF TABLES vii

LIST OF ILLUSTRATIONS viii

LIST OF SCHEMES xi

LIST OF ABBREVIATIONS xii

CHAPTER

I. INTRODUCTION 1

Brief Introduction of the Thesis
Quartz Crystal Microbalance with Dissipation Detector (QCM-D)
QCM-D Data Process

II. DENTAL CARE POLYMERS AND NATURAL DENTAL SURFACES 7

Maleic Anhydride Copolymers
Tooth Surface
Surface Adsorption of Polycarboxylates
Research Objectives

III. DENTAL MIMICKING SURFACES DEVELOPMENT 17

Chapter Overview
Experimental Details
Results and Discussion
Chapter Summary

IV. ADSORPTION KINETIC STUDIES OF GANTREZ® S-97 ON DENTAL MIMICKING SURFACES 33

Chapter Overview
Experimental Details
Results and Discussion
Chapter Summary

V. OIL SPILL AND OIL CLEAN-UP 50

Oil Spill and Its Effect to The Environment
Oil Spill Remediation Methods
Oil Dispersant with Anti-Deposition Function
Research Objectives

VI. OIL DISPERSANT WITH ANTI-DEPOSITION CAPABILITY AND ITS INTERACTION WITH A MODEL SANDSURFACE 58

Chapter Overview
Experimental
Results and Discussion
Chapter Summary

VII. CONCLUSIONS 70

VIII. RECOMMENDATIONS FOR FUTURE RESEARCH 73

REFERENCES 75

LIST OF TABLES

Table

1. Repeatability Testing of Water Contact Angle on the Nucleated CaP Layer.....28

2. CaP Layer Thickness Change During Washing Stability Testing.....28

3. CaP Layer Thickness and Water Contact Angle for Phosphoric (PA) Modified and CaP Coated Model Surfaces as a Function of Reaction Time of Phosphorylation 30

4. Changes in Frequency of The Third Overtone ($\Delta f3$) at the Equilibrium Stage of the Polymer Adsorption Process.....41

5. 10 Largest Oil Spill Accidents in History.....51

6. Thickness of Adsorbed Layers and Dimensions of Absorbed Oil Droplets.....68

LIST OF ILLUSTRATIONS

Figure

1. Diagram of Q-Sensor and a Schematic Illustration of the Strain Induced in an AT-Cut Crystal. 2

2. Typical QCM-D Traces: Adsorption of Gantrez S-97 BF on SiO_2 and Hydroxyapatite (HAp). The Shifted Frequency is Related to Adsorbed mass. 3

3. Typical QCM-D Traces: Adsorption of Gantrez S-97 BF on SiO_2 and Hydroxyapatite (HAp). The Change of Dissipation Rate Reveals the Structure of Adsorbed Layer. 4

4. QCM Traces of Gantrez® in 100 mM NaCl Solution at pH 7. The Frequency Decreases, and the Dissipation Increases as a Function of Time for Three Overtones (n=3, 5, and 7; f_0=5MHz) at 24±0.1 C. A 100 mM NaCl, pH 7 Rinse Solution (Containing No Polymer) was Injected at 1 h 4 min. 5

5. Structures of (a) Maleic Anhydride, (b) a MAn Copolymer and (c) a Hydrolyzed MAn Copolymer 7

6. Structures of Gantrez® Products 9

7. The Adsorption of Polyelectrolyte on the Oppositely Charged Surface. The Top Illustrates the Ionic Distribution when Polyelectrolyte is Approaching the Target Surface; the Bottom Illustrates the Corresponding Potential as a Function of Distance from the Surface. (Revised from Reference 31.) 11

8. Schematic of Electrophoretic Deposition 18

9. AFM Images of Gold Coated Si Wafer in Height Mode (a) and Phase (b) Mode. 23

10. Visual Comparison of the Bare Target Surface and the Modified Surface: (a) the Target Surface, Gold Coated Si Wafer; (b) the Modified Target Surface Deposited with HAp Nanoparticles Produced from Acid Base Synthesis. 23

11. ESEM Images of Modified HAp Surfaces Processed under 175 V DC Power with Different Reaction Times: (a) 30 s (Mag. 158X) ; (b) 60 s (Mag. 59X).....24

12. Visual Comparison of Bare Target Surface and the Modified Surface Prepared via Electrodeposition: (a) the Target Surface, Gold Coated Si Wafer; (b) the Modified Surface, Target Surface Deposited with HAp Nanoparticles from Metathesis Synthesis. 25

13. ESEM Images of Modified Surfaces Electrodeposited with HAp Nanoparticles from Metathesis Synthesis Processed under 175 V DC Power with Different Reaction Times: (a) 60 s; (b) 120 s. 26

14. Structure of Triethoxysilylpropyl Succinic Anhydride (TESPSA). 27

15. AFM Height Images of the 24 h Nucleation Modified CaP Surface: (a) before; and (b) after 10 min's Washing 29

16. QCM Traces of $CaCl_2$ 100 mM Solution. The Frequency Decreases, and The Dissipation Increases as a Function of Time for Three Overtones (n=3, 5, and 7; f_0=5MHz) at 24±0.1 C. Rinse Solution of DI Water was Injected at 1 h 25 min. 31

17. Representative QCM-D Traces for Polymer Adsorption on a HAp Coated QCM-D Slide: 0.05 mg/mL Gantrez® s 97 at pH 4.....37

18. Adsorption of Gantrez® s 97 from Solutions at Different Concentrations and pH Levels: (a) 0.2 mg/mL (below C*) at pH 4; (b) 0.2 mg/mL (below C*) at pH 7; (c) 5mg/mL (above C*) at pH 4; (d) 5mg/mL (above C*) at pH 7 as a Function of Time for Three Overtones (n=3, 5, and 7; f_0=5MHz) at 24±0.1 C. 39

19. Mass Uptake as a Function of Time for 0.2 and 5 mg/mL G-S97 Solutions at pH 4 and 7.....44

20. D-f plot for Adsorption and Desorption of (a) 0.2 mg/mL and (b) 5 mg/mL G-S97 Solutions at pH 4 and 7.....45

21. 3D AFM Images of pH Related Adsorption on CaP Model Surface (Left: Height, Right: Phase): (a) and (b) Blank CaP Model surface; (c) and (d) G-S97Adsorption at pH 4; (e) and (f) G-S97 Adsorption at pH 7. 47

22. Illustrations of Mechanical and Chemical Clean-up: (a) A US Navy oil spill response team drills with a "Harbour Buster high-speed oil containment system"; (b) A US Air Force Reserve plane sprays Corexit dispersant over the Deepwater Horizon oil spill in the Gulf of Mexico. Images are from Wikipedia[76]. As works of the U.S. federal government, the images are in the public domain. 52

23. Comparison of Oil Dispersant with and without Anti-Deposition Function: (a) without Stabilization the Dispersed Oil Still Has the Chance to Aggregate and to Deposit; (b) Polymeric Material Can Stabilize the Oil Droplet and Prevent the Redeposition. 54

24. Structure of (a) Soy Lecithin and (b) Hydroxypropyl Cellulose (HPC). 55

25. QCM Traces of Lecithin in Seawater. The Frequency Decreases (a) and the Dissipation Increases (b) as a Function of Time (in Seconds) for Three Overtones (n=3, 5, and 7; f_0=5MHz) at 24±0.1 C. 61

26. QCM Traces of HPC in Seawater. Very Little Change is Observed in Frequency (a) or Dissipation (b) as a Function of Time for Three Overtones (n=3, 5, and 7; f_0=5MHz) at 24±0.1 C.....62

27. QCM Traces of Oil and Lecithin in Seawater; the Frequency Decreases (a) and the Dissipation Increases (b) as a Function of Time for Three Overtones (n=3, 5, and 7; f_0=5MHz) at 24±0.1 C.....62

28. AFM Images of Oil and Lecithin on the Silicon Dioxide QCM Sensor in Height Mode (a) and Phase Mode (b).....63

29. QCM Traces of Oil and HPC in Seawater. There is No Obvious Change in Frequency (a) or Dissipation (b) as a Function of Time for Three Overtones (n=3, 5, and 7; f_0=5MHz) at 24±0.1 C.....64

30. Adsorption of Oil Lecithin and HPC, the Frequency Decreases (a) and The Dissipation Increases (b) as a Function of Time for Three Overtones (n=3, 5, and 7; f_0=5MHz) at 24±0.1 C. 65

31. AFM Height and Phase Images of Oil Lecithin and HPC Spread on the Silicon Dioxide QCM Sensors at Stage 1(a and b), Stage 2(c and d), and after Rinse by Seawater(e and f). 67

LIST OF SCHEMES

Scheme

1. Protonation and Deprotonation of Maleic Acid Moiety of G-S 97 upon pH Change....13

2. Schematic View of CaP Growth on Silanized Si Wafer....27

3. Development of Nanoscopically Smooth Model Dental Surface via Phosphorylation....30

4. Polymeric Adsorption and Desorption Processes for Polymer Layers Formed from High Concentration (above C*) G-S97Solutions: (a) Adsorbed Polymer was Covered by a Loosely Attached Viscous Layer; (b) Salt Solution Removed the Viscous Layer and (c) Adsorbed Polymer was Gradually Rinsed off by Ultra Pure Water....42

LIST OF ABBREVIATIONS

- AFM — Atomic force microscopy
- C* — Critical overlap concentration
- CaP — Calcium phosphate
- HAp — Hydroxyapatite
- HPC — Hydroxypropyl cellulose
- MAa — Maleic acid
- Man — Maleic anhydride
- G-S97 — Gantrez® S-97 BF, a poly(methyl vinyl ether-alt -maleic anhydride) copolymer
- pK_a — acid dissociation constant
- QCM-D — Quartz crystal microbalance with dissipation detector
- SBF — Simulated body fluid
- SDS — Sodium dodecyl sulfate
- TEM — Transmission electron microscopy
- TESPSA — Triethoxysilylpropyl succinic anhydride
- Δf — Frequency decrease in QCM-D traces
- ΔD — *Dissipation increase in QCM-D traces*

CHAPTER I

INTRODUCTION

Brief Introduction of the Thesis

This thesis involves two projects. The objectives of the first project were to 1) define an effective method to prepare a nanoscopically smooth dental mimicking surface and 2) determine the kinetics and adsorption/desorption behavior and morphology of adsorbed films of the dental care polymer Gantrez® S-97 BF (G-S97) (a poly(methyl vinyl ether-alt-maleic anhydride) copolymer) on dental mimicking surfaces as a function of solution properties. The goal of the second project was to determine the mechanisms and kinetics of adsorption/desorption properties of an oil dispersant based on hydroxypropyl cellulose and lecithin on a model sand surface. The unifying theme of this thesis is the description of stimuli-responsive polymer adsorption/desorption behavior on model surfaces designed to mimic natural surfaces. The goal is to develop a better understanding of the variables that govern polymer-surface interactions in aqueous solution in hope that the fundamental knowledge gained will be useful in developing and designing new polymer systems and formulations of biocompatible polymers for personal care and industrial applications. The primary techniques employed to determine the molecular-level mechanisms of adsorption and desorption are QCM-D and AFM. AFM is a well-known technique for evaluation of the morphology and nanomechanical properties of adsorbed polymer films.[1] The QCM-D methodology is briefly described.

Quartz Crystal Microbalance with Dissipation Detector (QCM-D)

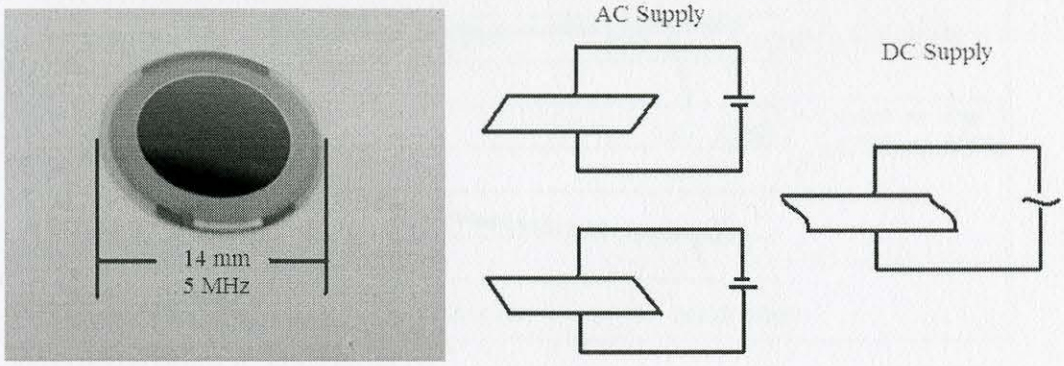

Figure 1. Diagram of q-sensor and a schematic illustration of the strain induced in an AT-cut crystal.

The QCM-D slide is a disk shaped piezoelectric quartz crystal sensor, which is usually sandwiched between two gold electrodes contacted with an electronic oscillator. When an AC voltage is applied across the electrodes, the crystal sensor oscillates at different frequencies. The quartz crystal can be coated with different materials to provide deposition surfaces for study of chemical and/or biological adsorption. During the adsorption process, changes in frequency (Δf) and dissipation factor (ΔD) caused by adsorbed materials on QCM-D slides are simultaneously recorded. The resonant frequency of the crystal, f, will decrease as the adsorbed mass (m) increases (Figure 2).

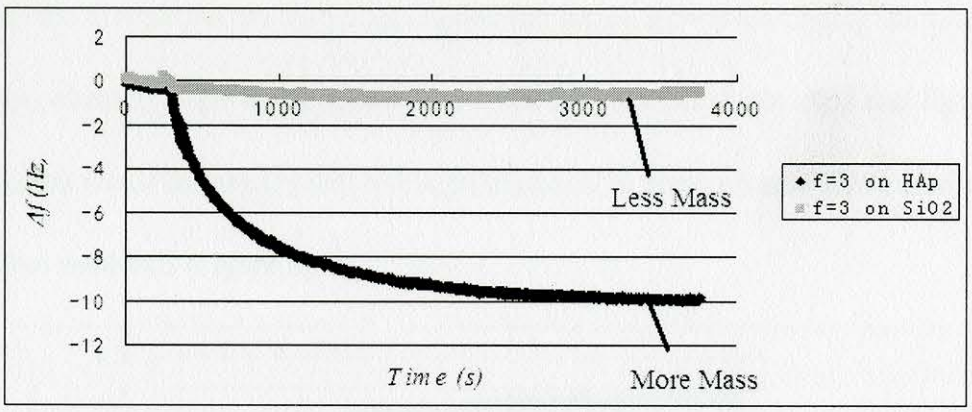

Figure 2. Typical QCM-D traces: Adsorption of Gantrez S-97 BF on SiO_2 and hydroxyapatite (HAp). The shifted frequency is related to adsorbed mass.

If the film is rigid, the frequency change $\Delta f = f_0 - f$, where f_0 is the resonant frequency of bare crystal in the medium, is proportional to the adsorbed mass. The relationship was described by Sauerbrey in 1959:[2]

$$\Delta m = -\frac{C\Delta f}{n} \qquad \text{(I-1)}$$

Where n is the overtone number (n=1, 3, 5, 7……) and C is the constant (C=0.177 mg m^{-2} Hz^{-1}) that reflects the sensitivity of the device to a change in mass. Since the AC voltage applied to the electrodes is operated intermittently, there is decay in oscillation due to energy losses. The dissipation factor D (unitless), which reflects the energy dissipation, provides information about the ratio of energy lost (E_{lost}) to the energy stored (E_{stored}) and is related to the time constant τ:[3,4]

$$D = \frac{E_{lost}}{2\pi E_{stored}} = \frac{R}{\omega L} = \omega RC = \frac{1}{\pi f \tau} \qquad \text{(I-2)}$$

Where f is the resonant frequency, and the angular frequency (ω) can be varied to determine the resistance (R), inductance (L), and capacitance (C) of the crystal. QCM-D

records the dissipation change in the dissipation factor: $\Delta D=D-D_0$ during the adsorption process, where D is the dissipation factor when the polymer is adsorbed and D_0 is the dissipation factor of bare crystal. ΔD is proportional to energy losses associated with the adsorbed materials (Figure 3).

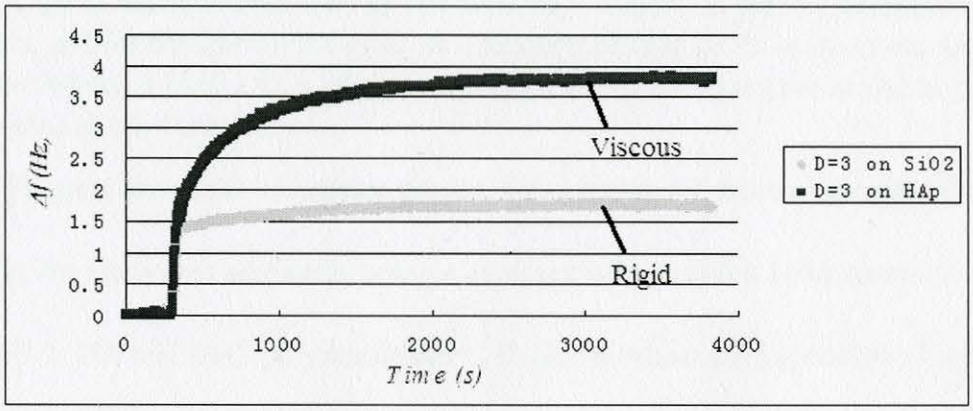

Figure 3. Typical QCM-D traces: Adsorption of Gantrez S-97 BF on SiO_2 and hydroxyapatite (HAp). The change of dissipation rate reveals the structure of adsorbed layer.

QCM-D Data Process

The commercial software, *Q-tools*, provides several models for QCM-D data process. The Sauerbrey model is used to calculate the adsorbed mass of the rigid layer. The Voigt model provides structural information, such as thickness, density and elasticity, for the solid viscous layer. The rigidity of the adsorbed layer can be judged by the performance of overtones; low ΔD (less than 10% of the frequency shift) and overlapping of overtones indicate the presence of a rigid layer.

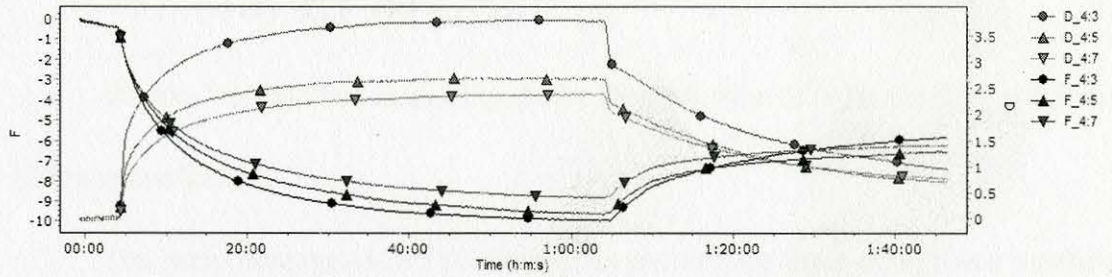

Figure 4. QCM traces of Gantrez® in 100 mM NaCl solution at pH 7. The frequency decreases, and the dissipation increases as a function of time for three overtones (n=3, 5, and 7; f_0=5MHz) at 24±0.1 C. A 100 mM NaCl, pH 7 rinse solution (containing no polymer) was injected at 1 h 4 min.

Figure 4 shows the adsorption profile of Gantrez® s97 solution monitored by QCM-D. The study was performed using a commercially available HAp coated Q-sensor with a pH 7, 100 mN NaCl polymer solution. High ΔD values and separation of the overtones are observed, indicating the non-rigid, viscoelastic nature of the adsorbed polymer layer.

The mass of the adsorbed viscous layer, which accounts both the adsorbed polymer and solvent, can be estimated from the density and thickness of the layer, or can be calculated using the Johannsmann model. The details of the Johannsmann model data process are described elsewhere.[5]

The diffusion coefficient is estimated from the initial portion of the adsorption curve. It is assumed that during the initial stage, when polymer adsorption is diffusion controlled, that each molecule that reaches the surface is adsorbed and the amount of adsorbed solvent can be ignored. Fickian diffusion is assumed in this short time period, and the diffusion coefficient is calculated by:[6]

$$\Gamma(t) = (2/\pi^{0.5})C_{bulk}(Dt)^{0.5} \qquad \text{(I-3)}$$

Where Γ is adsorbed mass, C_{bulk} is the concentration of bulk solution, and D is the diffusion coefficient.

The initial adsorption rate is obtained by plotting the mass change as a function of time, and the slope is the adsorption rate.

CHAPTER II

DENTAL CARE POLYMERS AND NATURAL DENTAL SURFACES

Maleic Anhydride Copolymers

Over the last two decades significant progress has been made in the development of biocompatible materials for applications including drug delivery, tissue engineering, and oral care.[7,8,9] Maleic anhydride copolymers are biocompatible and pH responsive and demonstrate strong interactions with biosurfaces.[10,11,12,13] The maleic anhydride (MAn) structure is shown in Figure 5.

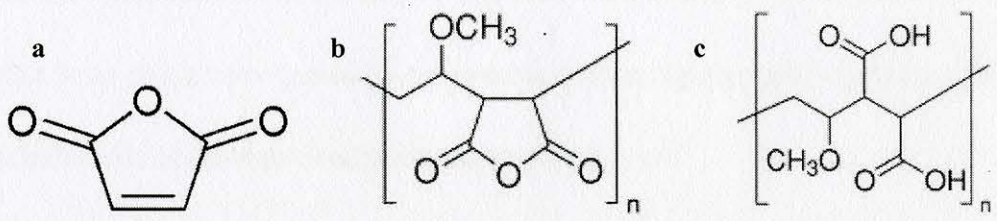

Figure 5. Structures of (a) maleic anhydride, (b) a MAn copolymer and (c) a hydrolyzed MAn copolymer.

MAn forms alternating copolymers with other monomers including styrene, 1-olefin, and vinyl ether. The excellent properties of MAn copolymers result from their structure. MAn groups hydrolyze partially or totally in water, providing water solubility to MAn copolymers. Additionally, the anhydride group in MAn copolymers can be used to bond with other compounds with a degradable ester or amide linkage, and after the reaction, there is still a carboxylate group remaining to maintain the water solubility of the polymer. This makes MAn useful in preparing drug delivery vehicles.[14,15,16] Maleic acid (MAa) groups possess two pKa's, with approximate values of pKa1=3.0 and

pKa2=6.2, which depend on the copolymer structure[17] and allow for the development of pH-responsive copolymers.

One area of intense research activity has been the use of MAn copolymers for oral care applications. Polymers containing carboxylate groups demonstrate dental adhesion properties, resulting from electrostatic interactions between carboxylic acid groups on the polymers and calcium ions on the tooth surface.[18] Due to their strong adhesion to the tooth surface, MAn copolymers have been used in the composition of denture adhesives, dental cements, and for the delivery of oral care components to the oral cavity.[19,20,21] Studies have also shown that MAn-vinyl methyl ether copolymers help reduce formation of calculus do not damage developing enamel surfaces.[21]

Gantrez® MA copolymers, a series of poly(methyl vinyl ether-*alt*-MA) copolymers produced by International Specialty Products Inc. (ISP®), are widely used for oral and personal care. The dental adhesion properties of Gantrez® have been primarily exploited for oral care applications, and the copolymer has been used as a dental coating and as the carrier for delivery of active ingredients such as flavor, antibiotic, or medicine in tooth paste and mouthwash.[22]

The Gantrez® product line of MAn copolymers and derivatives is generally divided into four families,[8] Gantrez® AN, Gantrez® S, Gantrez® MS, and Gantrez® ES, the structures of which are shown in Figure 6.

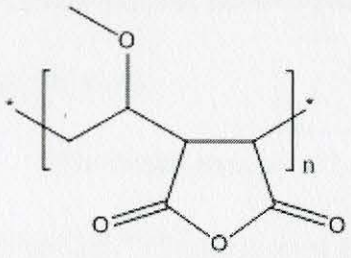

Gantrez® AN

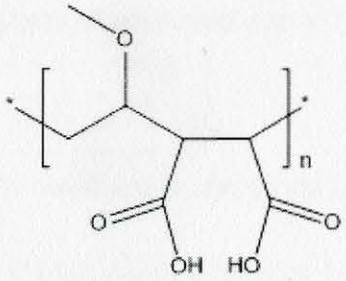

Gantrez® S

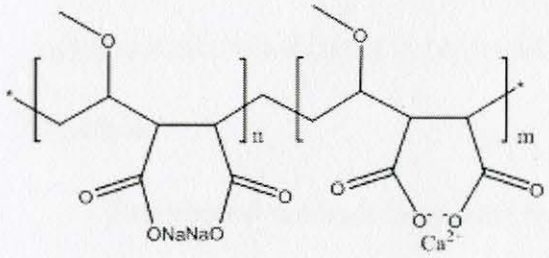

Gantrez® MS

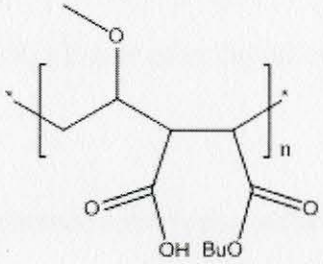

Gantrez® ES

Figure 6. Structures of Gantrez® products.

The most common interaction between Gantrez® and the oral cavity roots is the electrostatic attraction between carboxylate groups on the polymers and calcium ions on tooth surface. The adsorption of carboxylate ions on the tooth surface usually accompanies the release of phosphate and hydroxyl anions from the tooth. The adsorbed carboxylate may leave the tooth with calcium if the carboxylate calcium salt is water soluble.[23,24]

Tooth Surface

To gain an understanding of the mechanisms and stability of adhesion to the dental surface, it is of great interest to study the properties of the adsorbed polymer monolayer. The inhomogeneity of the natural surface presents a challenge to studying these interactions utilizing nanoprobe techniques. Thus, development of a

well-characterized, nanoscopically smooth model surface is an important part of the proposed study.

The dental enamel is the only exposed part of the tooth and is composed primarily of HAp/CaP.[25] HAp has poor mechanical properties and is not suitable for load-bearing applications.[26] The tooth surface has asperities in the scale of micrometers. At this roughness scale, it is difficult to observe the effects of polymer monolayers adsorbed to the surface.

Two general methods have been reported to prepare a substrate coated with a HAp/CaP layer. The first method includes an electron-beam deposition mechanism. HAp/CaP nanoparticles are first made, and then they are deposited onto a smooth substrate under a strong electrical field.[27,28] The second method, also known as chemical modification, uses a technique to create an environment that enables formation of a HAp/CaP layer on a substrate. These techniques include bio-nucleation coating[28] and phosphorylation coating.[29,30]

Surface Adsorption of Polycarboxylates

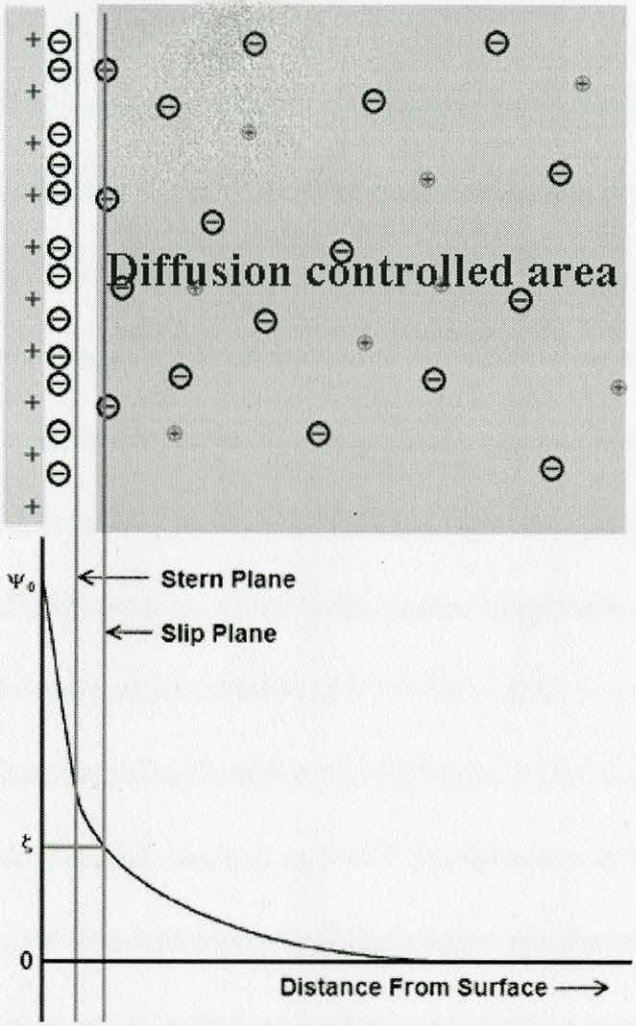

Figure 7. The adsorption of polyelectrolyte on the oppositely charged surface. The top illustrates the ionic distribution when polyelectrolyte is approaching the target surface; the bottom illustrates the corresponding potential as a function of distance from the surface. (Revised from Reference 31.)

The adsorption process of polycarboxylates on a charged surface can be described by a two-step mechanism.[31] When attaching to a surface, polymers first diffuse slowly to the proximity of the surface and then begin to interact with surface by both van der Waals force[32] and electrostatic interactions. Many variables may affect the adsorption behavior of polycarboxylates onto a charged solid surface, including solution conditions such as

pH, ionic strength, polymer concentration, and polymer structural parameters, including molecular weight and charge group distribution.

Altering the pH of the solvent affects the charge density of the polycarboxylate through protonation (or deprotonation) of the carboxylate anion. The screening effect of protons in solution may also influence the degree of repulsion between charged side groups and consequently change the conformation of the polyelectrolyte. High charge density polyelectrolytes exhibit extended conformations in aqueous solution, and when adsorbed on charged surfaces show extended, thin, monolayer morphologies.[33,34]

When small molecule salts are added to the aqueous polymer solution, adsorption onto a charged surface decreases dramatically at low concentrations of added salt. The decreased adsorption is attributed to the reduced electrostatic attraction between the carboxyl groups and the positively charged surface.[35] At higher concentrations of NaCl, significant increases in the absorbed mass of polycarboxylate are observed, attributed to the development of a more contracted polymer chain conformation in solution due to charge screening, which resulted in lower drag and deposition of a greater number of coiled polymer chains on the charged surface.[36,37]

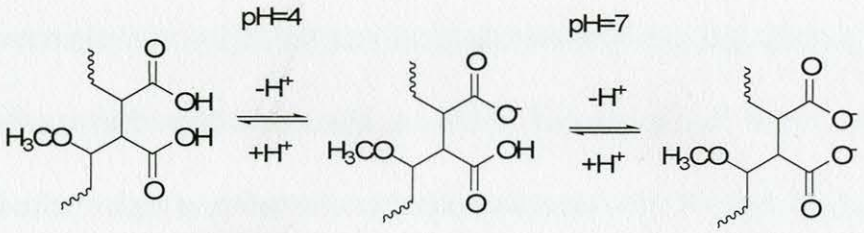

Scheme 1. Protonation and deprotonation of maleic acid moiety of G-S 97 upon pH change.

Knowledge of pK_a values is necessary for a quantitative understanding of the interaction between acids or bases and metal ions to form complexes (Scheme 1). In solutions with pH above pK_{a2}, the maleic acid copolymers with high charge density and high Gibbs free energy possess higher potential to form ionic bonds with metal ions than when the copolymers are in solution with pH below pK_{a1}. For polycarboxylates, conformational change would be expected if any chelation occurred between metal ions and the carboxyl groups along the polymer chain.[38,39]

The effect of polymer concentration on adsorption behavior is not a simple relationship. Some studies indicate that adsorption saturation is achieved only at or above a critical concentration, and below that concentration the adsorbed mass is proportional to the polymer concentration.[36,37] Few studies of the effect of concentration on adsorption rate of carboxylate polymers have been reported. Some studies of polyelectrolytes indicate that the initial rate of adsorption shows first-order dependence on the polyelectrolyte concentration within a specific range.[40] This dependence may be due to the fact that higher concentration increases the possibility of the formation of ionic bonds between the polyelectrolyte and the charged surface.

Lower molecular weight polymer molecules suffer lower drag when approaching the surface due to their smaller size, and as a result, they may adsorb faster. Adsorption of higher molecular weight polyelectrolytes is thermodynamically favored, because when the larger molecule replaces the preadsorbed lower molecular weight polymers, the released polymer will help to increase the number of polymer chains in solution and thus increase the entropy. This replacement is called the reconformation process.[31]

Most current theories assume that the polymer conformation in solution, as determined by polymer structure, solution pH, and salt concentration, determines the adsorption behavior on solid surfaces.[41,42,43] In general, MAn copolymers may exhibit contracted or extended conformations in aqueous solutions. At low pH, the carboxyl groups are protonated, and the polymers exist in coiled, relatively contracted conformations. At pH above pK_a, the carboxyl groups are deprotonated, and an extended conformation is observed due to charge-charge repulsion.[44,45,46,47,48] High salt concentration leads to contracted polymer conformation due to an electrostatic shielding effect. MAn copolymers with a high percentage of hydrophobic moieties form more contracted conformations than those with lower hydrophobic content.[49,50,51,52] It is predicted that MAn copolymers with contracted conformation in solution result in adsorbed films of higher mass and greater thickness on charged surfaces due to deposition in the more compacted structure, allowing attachment of a greater number of chains. MAn copolymers with extended conformations in solution usually display

adsorption of thinner films with lower mass due to the deposition of fewer, highly extended chains on the charged surface.

Research Objectives

The goal of this research is to study the polymer structural and solution factors controlling polymeric adsorption behaviors. Comprehensive studies of polymeric adsorption kinetics and adsorbed morphology on dental mimicking surfaces will provide further elucidation of the mechanisms involved in dental care polymer development.

In this study Gantrez® S-97 BF (G-S97), a free acid version of the Gantrez® series polymers, was selected as the model polymer. G-S97 is pH responsive and possesses two pKa's, with values of pK_{a1}=3.47 and pK_{a2}=6.47.[53]

The Objectives of this research are:

1. Define an effective method to prepare smooth HAp/CaP surfaces for morphology study. Complete comparative adsorption kinetics studies via Quartz Crystal Microbalance with Dissipation Detector (QCM-D) with G-S97.
2. Investigate the effects of solution properties (concentration, ionic strength, and pH) on polymeric adsorption behavior on the model HAp surface.
    a) Study the kinetics of adsorption as a function of copolymer structure and solution conditions using QCM-D analysis.
    b) Determine the morphology and thickness of adsorbed layers on the HAp model surface utilizing AFM and ellipsometry.

3. Delineate the mechanisms of maleic anhydride copolymer adsorption on model surfaces to provide information for design of systems for biomedical and personal applications.

CHAPTER III

DENTAL MIMICKING SURFACES DEVELOPMENT

Chapter Overview

Three methods were attempted to develop a nanoscopically smooth model dental surface for polymer morphology studies. Surfaces were modified with HAp-mimicking films. Film thickness and roughness were evaluated by ellipsometry and microscopy techniques. The reproducibility and the stability of the modified surfaces were determined. A phosphorylation technique was shown to be the most promising for continued study.

Experimental Details

Cleaning of Si Wafers

Cleaned Si wafers were used as substrates to develop smooth dental mimicking surfaces. Silicon wafers (Silicon Inc. Boise, Idaho, USA) were cut into 12×12 mm^2 pieces and all pieces, were treated with piranha solution (25% H_2SO_4, 75% H_2O_2) for 30 min, then immersed in 18.2 MΩ cm ultra pure water for 20 min. And then dried with a slow stream of N_2.

Electrophoretic Deposition

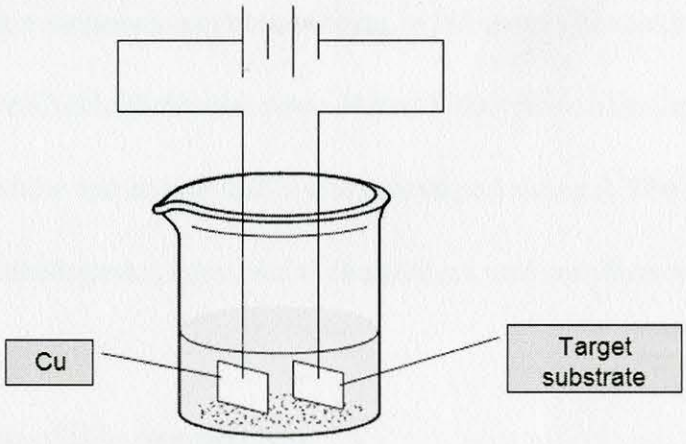

Figure 8. Schematic of electrophoretic deposition.

The electrophoretic deposition procedure followed a method reported by Wei and coworkers.[27] The equipment for electrophoretic deposition iss displayed in Figure 8. The beaker was filled with an ethanol suspension of Hap, and the target surface was a cleaned Si wafer coated with a thin layer of gold. The coating of gold was achieved using an Emitech K550X gold sputter coater under an argon atmosphere, and the coating time was 30 s or less. The two electrodes were connected to a high voltage power supply (Model REG-250-0.3, Matsusada Precision Inc., Japan). The deposition parameter (voltage and time) was controlled at different levels. The distance between the two electrodes was 6 mm. To ensure high efficiency of the deposition, the copper electrode was polished using abrasive paper before use.

Acid Base Synthesis of HAp Nano Particles

5.0 g $Ca(OH)_2$ (≥95%, Sigma Aldrich Co. USA) was dissolved in 200 mL DI water with continuous magnetic stirring. This was named solution A. A saturated solution

comprising 8.6 g K_3PO_4 (≥98%, Sigma Aldrich Co. USA) in DI water was slowly added into solution A with continuous magnetic stirring. A pH meter (Accumet AR50 Dual Channel pH/mV/Ion/Conductivity Benchtop Meter, Fisher Scientific Co. USA) was used to monitor the pH value and ensure that it was maintained above 7. The precipate was isolated through centrifugation, supernatant decantation, and was then resuspended in DI water.

Metathesis Synthesis of HAp Nanoparticles

47.22 g $Ca(NO_3)_2 \cdot 4H_2O$ (≥99%, Sigma Aldrich Co. USA) was added into 180 mL dilute ammonia DI water solution with continuous magnetic stirring. The pH value of the solution was adjusted to 12 with an ammonia saturated solution and then 180 mL DI water was added. The aforementioned solution was named solution B. 15.84 g $(NH_4)_2HPO_4$ was added into 450 mL of an ammonia solution (ammonia:DI water=1:2) with continuous magnetic stirring. The pH of this solution was adjusted to 12 and then mixed with 190 mL DI water. This was named solution C. Solution D was then slowly added into solution B at a rate of 100 mL/min with continuous magnetic stirring. The resulting suspension was heated to boiling point and stirred at boiling point for 1h. The suspension was then cooled to room temperature and aged for 3 weeks. The precipate was isolated through centrifugation, supernatant decantation, and was then resuspended in DI water.

Nucleation Growth of $CaPO_4$ on Silanized Silicon Wafer

The procedure to grow $CaPO_4$ on a silanized silicon wafer followed a method reported by Toworfe.[29] Cleaned Si wafers were treated with UV-ozone using a Bioforce Nanoscience UV Ozone ProCleaner™ for 10 minutes to oxidize the surface. After, UV-ozone treatment surfaces were treated with triethoxysilylpropyl succinic anhydride (TESPSA) under nitrogen for ~16 h at room temperature. Then, the reaction samples were ultra-sonicated serially in toluene, DMF (N, N-dimethlyformamide), and ultra-pure water for 20 min each and dried under nitrogen. .

Simulated body fluid (SBF) was used for in-vitro growth of $CaPO_4$ on silanized surfaces. SBF was prepared using a mixture of salts: NaCl (0.11 mol), $NaHCO_3$ (4.8 mmol), KCl (2.8 mmol), K_2HPO_4. $3H_2O$ (1.10 mmol), $MgCl_2.6H_2O$ (1.7 mmol), $CaCl_2$ (2.6 mmol), Na_2SO_4 (0.07 mmol), HCl (1M, 1mL), and $(CH_2OH)_3CNH_2$ (0.05mol). Salts were dissolved in ultra pure water (100 mL), and pH was adjusted to 7.4 using 1M NaOH. Silanized silicon wafers were immersed in SBF at different time intervals to induce the growth of CaP.

CaP Growth on Phosphorylated Si Wafer

The cleaned substrates were immersed into a mixed solution containing 10 mM phosphorus oxychloride ($POCl_3$) and 10 mM 2,4,6-collidine in acetonitrile at 70°C for 12 h and 24 h, respectively. The modified substrates were placed into a 0.5 mM $CaCl_2$ solution for 20 min. The thickness changes after each step were monitored by ellipsometry.

Ellipsometry

Ellipsometry was employed to monitor the thickness change of the dental mimicking surface during the phosphorylation and the nucleation process. The ellipsometric measurements were performed using a Gaertner Scientific ellipsometer (632.8 nm helium-neon laser source) with an angle of incidence of 70°. The phase difference (Δ) were collected, and the thicknesses were determined via ELLI software using refractive indices of each of the ellipsometry measured layers. Refractive indices of 3.89 for silicon, 1.46 for silicon oxide, and 1.441 for TESPSA were used.

Water contact angle

Water contact angle measurements were conducted to monitor the surface modification behaviors of the dental mimicking surfaces. The measurements were performed on a Rame-Hart goniometer coupled with DROP-image® data analysis software, employing the sessile drop technique. The static contact angle formed by drops of HPLC grade water (8μL) on the dental mimicking was measured immediately after deposition.

Results and Discussion

As mentioned above in Chapter II, there are several methods reported to prepare a CaP/HAp layer on a smooth substrate. Although pulse laser spraying is one of the most efficient ways to deposit HAp particles to a target surface, the roughness of the resulting modified surface is very high. Even after thermal polishing and annealing, the reported roughness is in the range of hundreds of nanometers to several micrometers, which is

dramatically higher than our target surface roughness (< 5 nm).[27,28] With the goal of obtaining a nanoscopically smooth model Hap surface for evaluation of the morphology of adsorbed polymer thin films, attempts were made to employ electrophoretic deposition, CaP nucleation, and phosphorylation.

Electrophoretic deposition

The electrophoretic deposition of HAp nanoparticles onto metal surfaces was reported by Wei and coworkers.[27] The details of the electrophoretic deposition were detailed in the experimental section of this chapter. It needs to be pointed out that the power resource must be a DC power supply which can provide high voltage (over 100 V). An AC power or lower voltage of DC may not induce the electro-deposition process.

In order to obtain a smooth dental mimicking surface, a gold coated Si wafer was employed as the deposition target for HAp nanoparticles in this research. Attempts to use both a sputterer and a thermal evaporator to coat a thin layer of gold on cleaned Si wafers were made, and according to AFM measurement, a smooth substrate (RMS=1.16 nm) was obtained by controlling the sputtering time within 30 s (Figure 9).

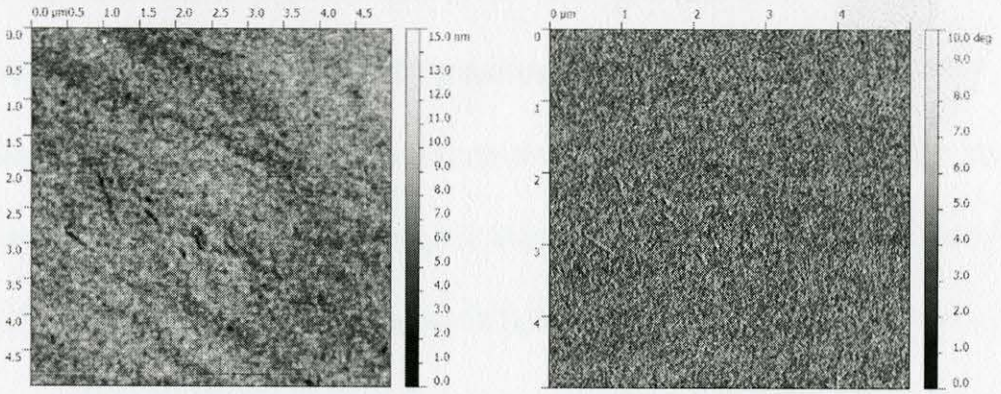

(a) (b)

Figure 9. AFM images of gold coated Si wafer in height mode (a) and phase (b) mode.

HAp nanoparticles prepared from two methods (acid base synthesis and metathesis synthesis) were used for electrophoretic deposition. The modified surfaces were tested visually and by using ESEM and AFM.

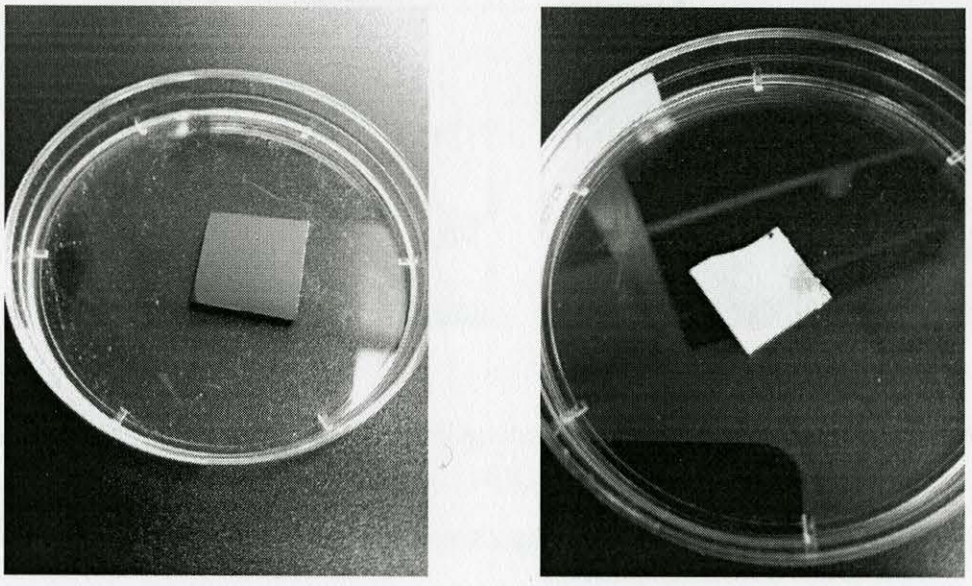

(a) (b)

Figure 10. Visual comparison of the bare target surface and the modified surface: (a) the target surface, gold coated Si wafer; (b) the modified target surface deposited with HAp nanoparticles produced from acid base synthesis.

Figure 10 shows the gold coated Si wafer (the target surface for deposition) and the modified surface developed with HAp nanoparticles produced from acid base synthesis. A thick and opaque layer was formed on the target substrate. The HAp layer demonstrated very poor stability during a scratching test. Some powder-like HAp was observed to fall from the surface with even a light touch of a knife. The effects of voltage and reaction time on electrophoretic deposition were investigated. The voltage was varied from 0 V to 200 V, and it was found an efficient deposition was not achieved until the voltage reached 160 V. Once induced, the deposition proceeded quickly (within a few seconds).

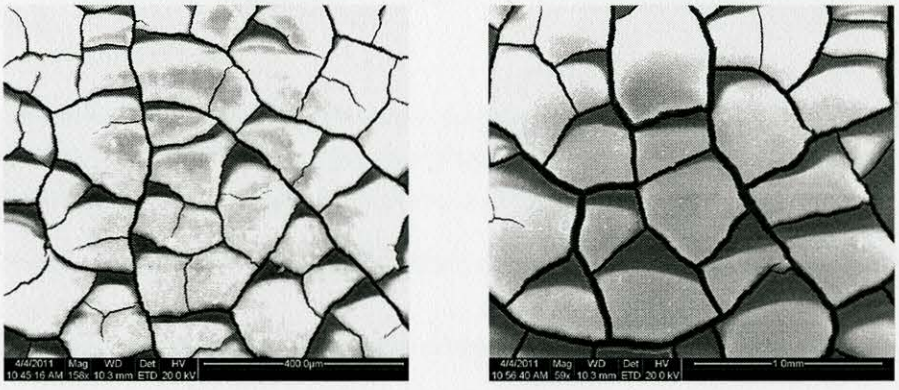

(a) (b)

Figure 11. ESEM images of modified HAp surfaces processed under 175 V DC power with different reaction times: (a) 30 s (Mag. 158X); (b) 60 s (Mag. 59X).

Figure 11 shows ESEM images of samples prepared by electrodeposition of HAp particles produced by acid base synthesis at different reaction times. Both surfaces are non-uniform and discontinuous with large cracks. The cracking was assumed to be caused by the fast evaporation of ethanol. However, even if the developed surfaces were

dried in an ethanol vapor environment, the HAp layer still cracked. AFM imaging was attempted on flat portions of the films away from the cracked areas; however, the roughness was too great to obtain images.

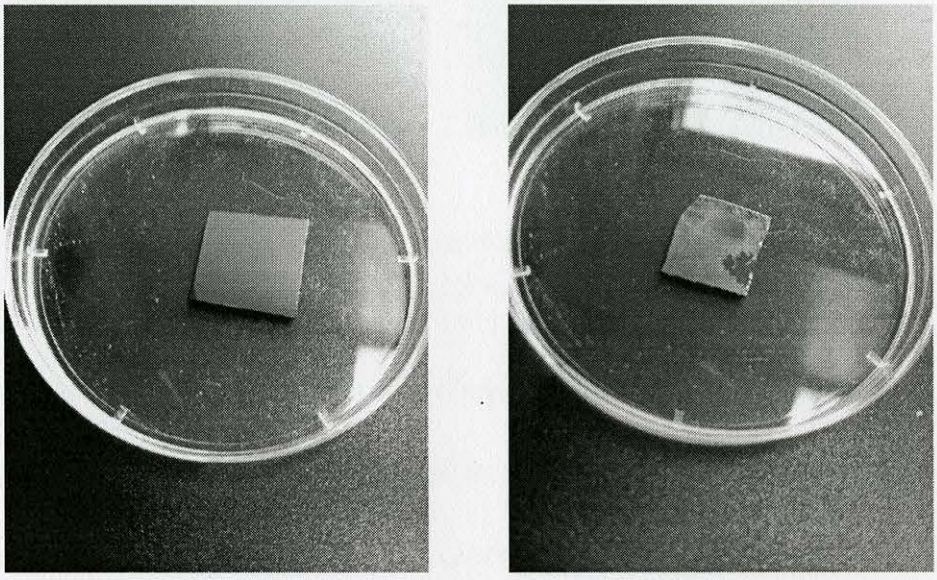

(a) (b)

Figure 12. Visual comparison of bare target surface and the modified surface prepared via electrodeposition: (a) the target surface, gold coated Si wafer; (b) the modified surface, target surface deposited with HAp nanoparticles from metathesis synthesis.

The electrodeposition modified surface deposited with HAp nanoparticles obtained via metathesis synthesis was also compared with the gold coated Si wafer (target substrate for deposition). A thin and transparent HAp layer was formed on the target surface after electrodeposition. Scratch testing of the deposited film revealed that it was possible to remove a section of the coating only with hard scratching, indicating increased stability of the layer (shown in Figure 12b). The effects of voltage and reaction time on electrophoretic deposition were also investigated. The voltage was varied from 0 V to 200 V, and there was no limitation of voltage was observed.

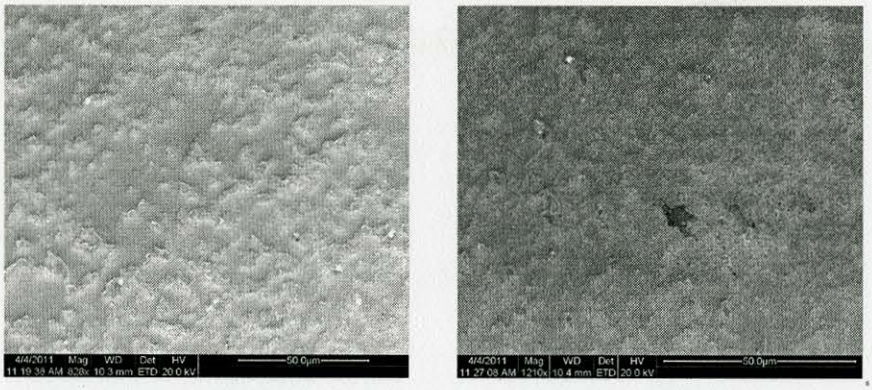

(a) (b)

Figure 13. ESEM images of modified surfaces electrodeposited with HAp nanoparticles from metathesis synthesis processed under 175 V DC power with different reaction times: (a) 60 s; (b) 120 s.

Figure 13 shows ESEM images of surfaces on which Hap nanoparticles prepared by metathesis synthesis were electrodeposited for different reaction times. For both samples, a uniform film is observed with no apparent cracking on the surface; raised features are attributed to nanoparticle aggregates. In the sample prepared with 60 seconds of reaction time, rod-like structures with lengths of tens of microns are observed. With increased reaction time (~120 s), aggregates appear smaller and rod-like features are not observed. AFM analysis revealed the roughness of the film produced after 60 seconds of reaction and that produced with 120 seconds of reaction was still too high for AFM imaging.

CaP Nucleation on Silanized Silicon Wafer

Previous work in the laboratories indicated that nucleation and growth of CaP on a silanized Si wafer is a potential method to develop a nanoscopically smooth model surface. Yuhong Wei reviewed this method and discussed the effect of the organosilane functional group on CaP nucleation.[54] This thesis will focus on the feasibility of

employing this method to produce a nanoscopically smooth dental mimicking surface for polymer adsorption studies.

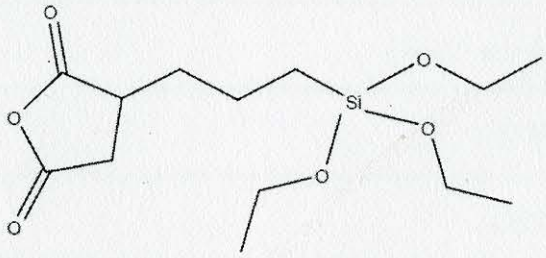

Figure 14. Structure of triethoxysilylpropyl succinic anhydride (TESPSA).

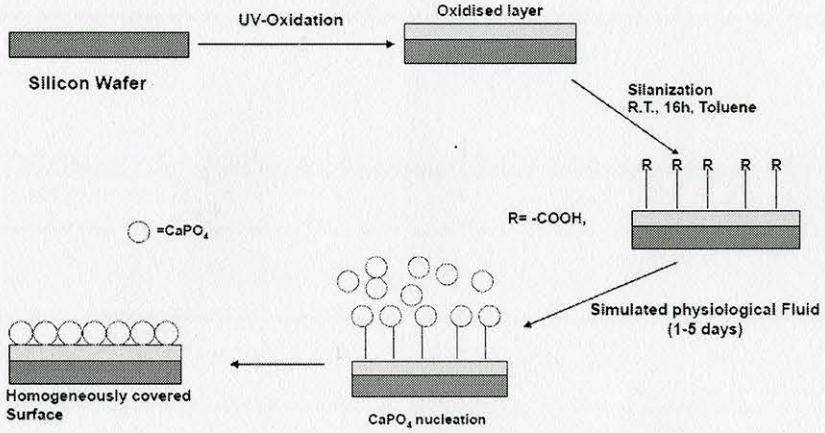

Scheme 2. Schematic view of CaP growth on silanized Si wafer.

The silane selected for Si wafer modification was triethoxysilylpropyl succinic anhydride (TESPSA, structure was shown in Figure 14). Scheme 2 provides a schematic view of Si wafer modification as well as the nucleation process to develop the CaP layer.

The results of repeated studies and stability of the CaP layer after washing in DI water for different periods of time are summarized in Table 1. Similar water contact angles and thicknesses were achieved for the three replicates where CaP nucleation proceeded for 48 hours. The CaP layers were approximately 120 – 150 nm thick, which exceeds the limitation for accurate measurement by the ellipsometer (Table 2).

Table 1

Repeatability Testing of Water Contact Angle on the Nucleated CaP Layer

	Water contact angle (°)
Repeat 1	47.8±0.9
Repeat 2	50.5±1.1
Repeat 3	49.2±1.1

Table 2

CaP Layer Thickness Change During Washing Stability Testing. (unit: nm)

0 min	*1 min*	*5 min*	*24 h*
> 100	49.6	7.9	6.9
> 100	20.5	5.6	5.3
> 100	36.6	5.9	5.4

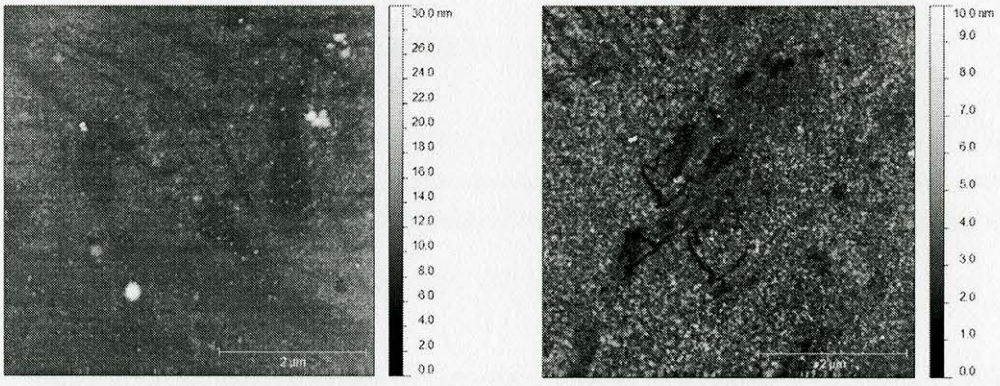

(a) (b)

Figure 15. AFM height images of the 24 h nucleation modified CaP surface: (a) before; and (b) after 10 min's washing.

To evaluate the stability of the CaP films, the samples were immersed in water in scintillation vials and placed on a shaker for 1 min, 5 min, and 24 hours, and the thickness was analyzed. After five minutes of immersion, the film thickness was reduced from over 100 nm to 5 – 7 nm, and it appeared fairly stable beyond this time. Figure 15 displays AFM images of the CaP surfaces after washing tests. It appears that large CaP particles were removed after washing, and the film washed for ten minutes is no longer continuous. Also, it was observed that water contact angle increased from 51.4±2.5°to 55.0±2.5°after washing 10 min. It was concluded that the relatively poor washing stability of the CaP layer formed by nucleation on the silanized silicon wafer would limit its usefulness as a dental mimicking surface.

CaP Growth on Phosphorylated Si Wafer

We developed a nanoscopically smooth model dental surface for AFM analysis using a modified phosphorylation approach, following that reported by Kim et al. as

shown in Scheme 3.30. The thin layer of calcium phosphate provides a model surface to mimic the composition of the tooth surface.

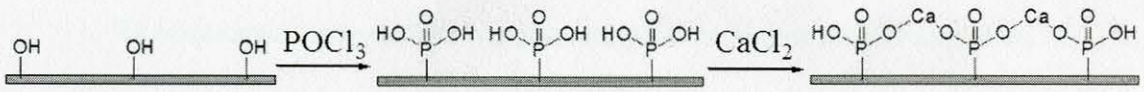

Scheme 3. Development of nanoscopically smooth model dental surface via phosphorylation.

Table 3 shows the thickness of the coating layer (measured by ellipsometry) as a function of reaction time and water contact angle of the surface for each step of the phosphorylation process.

Table 3

CaP Layer Thickness and Water Contact Angle for Phosphoric (PA) Modified and CaP Coated Model Surfaces as a Function of Reaction Time of Phosphorylation.

Reaction time	CaP layer thickness* (nm)	Water contact angle of PA modified surface± (°)	Water contact angle of CaP covered surface (°)
12 h	0.2±0.1	34.8±1.8	25.1±4.3
24 h	0.7±0.1	52.4±2.4	31.2±3.9

* Measured by ellipsometry

± Cleaned silicon wafer is completely water wetting

The thickness of the CaP layer was found to be 0.2 nm after 12 h reaction and 0.7 nm for 24 h reaction. Longer reaction time may increase the roughness of the surface and

result in larger measured contact angle. The incorporation of calcium in the phosphoric acid coating was indicated by the change in water contact angle.

The reproducibility and washing stability of the CaP layer developed by this method was also tested. Ellipsometry results indicated that for 3 replicates the thickness of the CaP layer was on average 0.7±0.1 nm after 24 hr reaction time. The washing stability test was performed using QCM-D evaluation. In this experiment, $CaCl_2$ solution was injected and flowed on a phosphorylated silicon coated QCM-D slide to attempt to grow a CaP layer as shown in Figure 16.

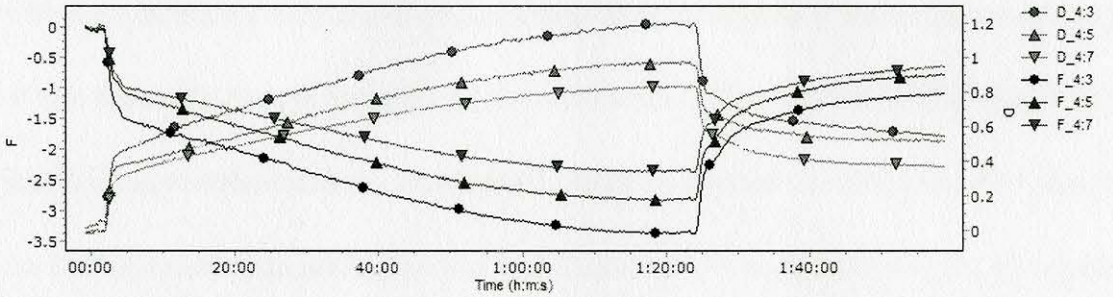

Figure 16. QCM traces of $CaCl_2$ 100 mM solution. The frequency decreases, and the dissipation increases as a function of time for three overtones (n=3, 5, and 7; f_0=5MHz) at 24±0.1 C. Rinse solution of DI water was injected at 1 h 25 min.

It is clear that Ca^{2+} attached to the surface in a short period of time by the decrease in frequency ($\Delta f3$=-1 Hz), and the corresponding thickness was 0.7 nm. This process is regarded as the formation of a firmly attached CaP layer. With the continued pumping of the $CaCl_2$ solution, the frequency continued to decrease and became stable after 1h and 20 min, which was attributed to the attachment of free Ca^{2+} onto the surface. The calculated thickness reached a peak value of 1.5 nm at 1h and 25min. After the stable baseline was achieved, DI water was injected to rinse the surface. The frequency then

increased, and a second stable baseline was achieved, which corresponded to a calculated thickness of 0.6 nm similar to that measured in the first five minutes of testing. It was concluded that a stable CaP layer of thickness 0.7±0.1 nm was formed that was resistant to removal by water. The QCM-D results are consistent with the ellipsometry measurements.

Chapter Summary

Three methods were employed to attempt to develop a dental mimicking surface for polymer morphology studies. The electrophoretic deposition method produced films with high efficiency, but the surface roughness was too high to evaluate the morphology of thin films adsorbed to the surface. The nucleation of CaP onto a silanized silicon wafer produced a nanoscopically smooth dental mimicking surface. However, the thickness of the CaP layer reduced quickly from over 100 nm to 5~7 nm with only 5 minutes exposure to DI water. The relatively poor stability of the CaP layer formed on silanized Si wafer would limit its usefulness as a dental mimicking surface. The CaP dental mimicking surface based on the phosphorylation of a modified Si wafer showed very low roughness (~0.3 nm). QCM-D measurements indicated the CaP layer was stable to DI water rinsing. Because of its reproducibility, stability, and production of a nanoscopically smooth CaP surface, the phosphorylation method was selected to produce the model dental surface for subsequent testing.

CHAPTER IV

ADSORPTION KINETIC STUDIES OF GANTREZ® S-97 ON DENTAL MIMICKING SURFACES

Chapter Overview

In this study, HAp coated QCM-D slides (to simulate dental surfaces) were used to evaluate G–S97 adsorption/desorption processes and kinetics for solutions of varying polymer concentration and pH. To further elucidate the mechanisms of adsorption for these polymers, the morphology of thin films produced from the solutions were analyzed using AFM. Phosphorylation of a cleaned silicon wafer was employed to provide a thin film of CaP to mimic the dental enamel surface. This smooth CaP surface allowed determination of the structure for the thin films produced from adsorption of polymer from solutions of varying concentration and pH to complement the QCM-D studies. Ellipsometry evaluation provided information about the thickness of the adsorbed films, and solution viscosity studies were performed to determine the critical overlap concentration of the polymer in solutions of varying pH.

Experimental Details

Materials

Gantrez® S97 (G-S97) was kindly provided by ISP technologies, Inc., Wayne, NJ, USA. Sodium chloride (NaCl, ≥99.5%) was purchased from Sigma-Aldrich. All chemicals were used as received. 100 mM NaCl solution, which was used as the solution for all polymer samples, was prepared by dissolving NaCl in 18.2 MΩ cm ultra pure

water. G-S97 solutions of desired concentrations were prepared in the aforementioned NaCl solution, and the pH was adjusted using NaOH.

Substrates for QCM-D Studies

The QCM-D slides used were quartz crystal sensors, an AT-cut piezoelectric quartz crystal 14 mm in diameter and 0.3 mm in thickness coated with a 10nm thick hydroxyapatite layer (QSX 327, Biolin Scientific, Inc. Linthicum Heights, MD, USA). Before performing QCM analysis, all QCM-D slides were cleaned using UV/ozone treatment for 15 min, followed by immersion in a solution of 2% sodium dodecyl sulfate (SDS) in 18.2 MΩ cm ultra pure water for 30 min at room temperature. The slides were then rinsed with 18.2 MΩ cm ultra pure water and further cleaned using UV/ozone treatment for 10 min.

Quartz Crystal Microbalance with Dissipation Monitoring (QCM-D)

In this study a QCM-D E4 system (Q-sense Inc., Gothenburg, Sweden) was used at 24±1 ℃ to monitor both adsorption and desorption of G S97 on a HAp surface. For the QCM-D study, solutions were prepared at concentrations of 0.05, 0.2, 1, 4, and 5 mg/mL at both pH 4 and 7. 100 mM NaCl solution and 18.2 MΩ cm ultra pure water were used to rinse adsorbed samples once the adsorption/desorption process reached equilibrium state (as defined by formation of a stable baseline). Four separate resonant frequencies (overtones, n) were used to drive oscillation of the shear wave through the sensor crystal. The changes in frequency (Δf) and dissipation factor (ΔD) were recorded simultaneously as a function of time at 5 MHz (fundamental overtone, n =1), 15 MHz

(n=3), 25 MHz (n =5), and 35 MHz (n =7). Since the noise at 5 MHz was very large, the data on fundamental overtone (n=1) was neglected, as reported previously by other researchers.[55,56] Each measurement was repeated at least two times. The maximum change in Δf was repeatable to within ±0.5 Hz and that of ΔD to within $\pm 0.2\times10^{-6}$.

Substrates for AFM Measurements

A nanoscopically smooth model dental surface was developed following a modification of the phosphorylation approach reported by Kim et al.[30] Silicon wafers (Silicon Inc. Boise, Idaho, USA) were cut into 12×12 mm^2 pieces to use as substrates for further development. Before modification, all pieces were treated with piranha solution (25% H_2SO_4, 75% H_2O_2) for 30 min, then immersed in 18.2 MΩ cm ultra pure water for 20 min and then dried with a slow stream of N_2. The cleaned substrates were immersed into a mixed solution containing 10 mM phosphorus oxychloride ($POCl_3$) and 10 mM 2,4,6-collidine in acetonitrile at 70°C for 12 h and 24 h, respectively. The modified substrates were placed into a 0.5 mM $CaCl_2$ solution for 20 min. The thickness changes after each step were monitored by ellipsometry.

Atomic Force Microscopy

The morphology of adsorbed G-S97 samples was investigated by AFM (Digital Instruments, Santa Barbara, CA: Dimension 3000) in tapping mode. A silicon probe (Veeco, Camarillo, CA) with a nominal force constant of 40 N/m and resonance frequency of 335–345 kHz was used to image all samples. AFM images were taken at a scanning size of 0.5×0.5 μm^2, and the resolution was held constant at 512×512 data

points. Both height and phase images were collected simultaneously. AFM images were taken in air in a temperature (25°C) and humidity (50%) controlled room and were processed using Gwyddion v2.30 software. At least three macroscopically separated areas were imaged for each sample, and the representative images are displayed. The image root-mean-square (rms) roughness is calculated as the root-mean-square average of the height deviations taken from the mean data plane, according to Equation 3[57]

$$R_{rms} = \sqrt{\frac{1}{N}\sum_{j=1}^{N} r_j^2} \qquad \text{(IV-1)}$$

where N is the total number of pixels and r_j is the vertical distance of pixel *j* from the mean surface-height plane.

To prepare the samples for AFM study, model dental surfaces were immersed for 3 h in 5 mg/mL G S97 solutions of pH 4 and pH 7. The substrates were then quickly dipped in 18.2 MΩ cm ultra pure water to remove salt and dried with a weak stream of nitrogen.

Intrinsic Viscosity

Preliminary intrinsic viscosity measurements and results were reported by Yuhong Wei in her thesis.[54] Generally, intrinsic viscosity ($[\eta]$) measurements were used to estimate the critical overlap concentration ($C^* = 1/[\eta]$) of the polymer solutions. The apparent viscosities of G-S97solutions were measured using an Ubbelohde viscometer at five different concentrations. For each concentration, inherent viscosity, $\ln(\eta/\eta_0)/c$, and

reduced viscosity, η_{sp}/c, were calculated from the apparent viscosity measurements and plotted against polymer concentration to prepare a Huggins-Kraemer plot.[58] Intrinsic viscosity was calculated from the extrapolation of the plots to the Y intercept.

Ellipsometry and Water Contact Angle

Ellipsometry and water contact angle goniometry experimental details are provided in Chapter III.

Results and Discussion

Quartz Crystal Microscopy Analysis of the Adsorption Process

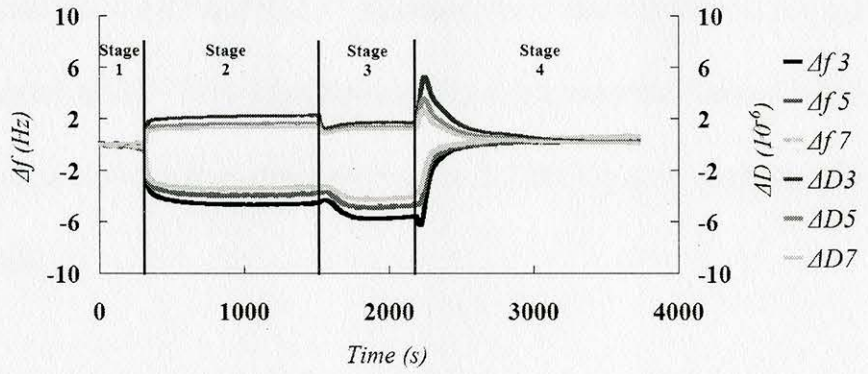

Figure 17. Representative QCM-D traces for polymer adsorption on a HAp coated QCM-D slide: 0.05 mg/mL Gantrez® s 97 at pH 4.

The adsorption of G-S97 onto hydroxyapatite coated surfaces was evaluated as a function of solution pH and polymer concentration using QCM-D. The experiments were conducted in four stages, as illustrated in Figure 17. First, 100mM NaCl stock solution was pumped over the HAp coated QCM-D slides until a stable baseline was obtained, where no change in frequency *(f)* or dissipation factor *(D)* was observed. In the second stage, polymer solution was injected into the flow line and pumped at a steady rate until a

second stable baseline was observed, assumed to be the point at which the maximum level of polymer adsorption to the substrate was achieved. In the third step, a 100 mM NaCl rinse solution was pumped through the system to remove any loosely associated polymer from the adsorbed layer. Finally, a DI water rinse was applied and a final baseline recorded. A decrease in f is related to an increase in adsorbed mass, while an increase in D is related to an increase in the viscoelastic response of the adsorbed polymer.[2-4]

Polymer solutions of five different concentrations were evaluated. The critical overlap concentrations (C*s) of G-S97 solutions were determined to be 3.3 mg/mL at pH 4 and 2.4 mg/mL at pH 7 from intrinsic viscosity measurements. Thus, three solutions were prepared at concentrations below C* (0.05, 0.2 and 1mg/mL) and two above C* (4 and 5 mg/mL).

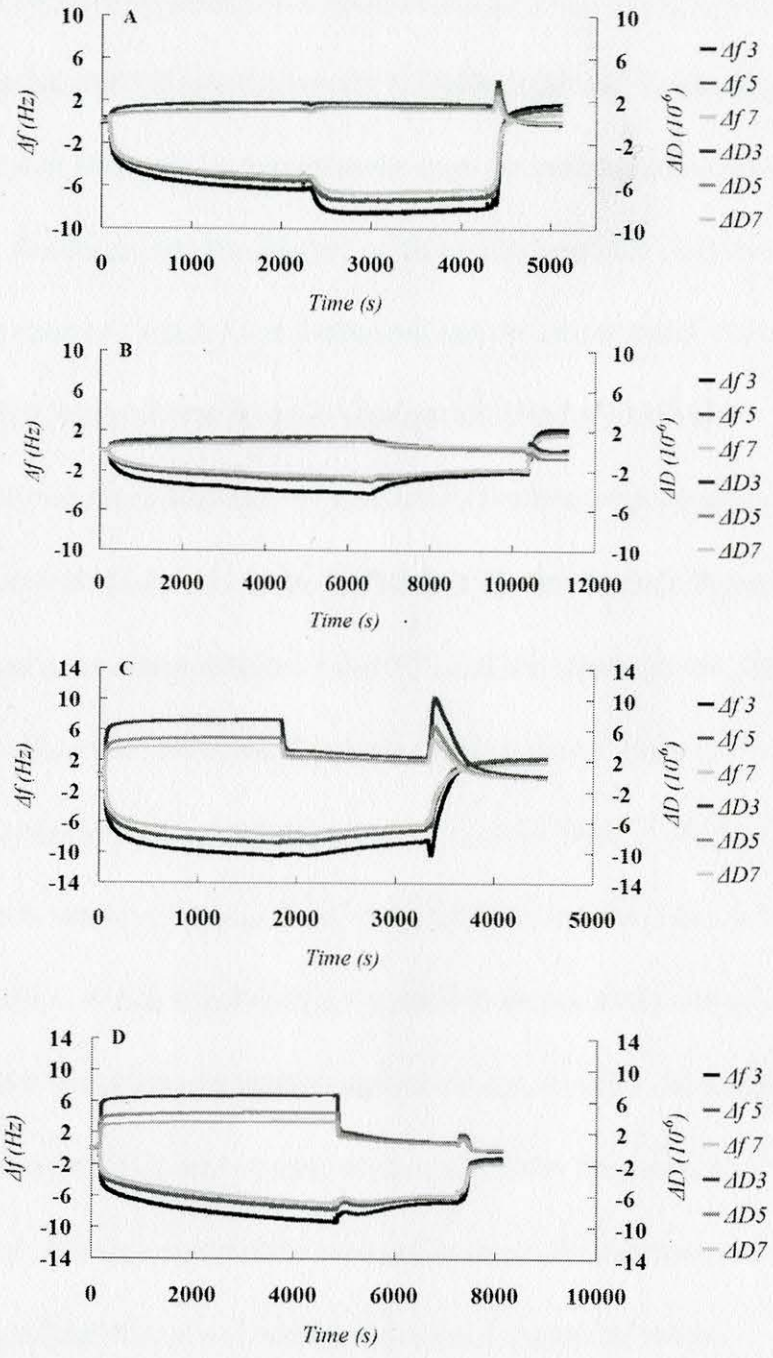

Figure 18. Adsorption of Gantrez® s 97 from solutions at different concentrations and pH levels: (a) 0.2 mg/mL (below C*) at pH 4; (b) 0.2 mg/mL (below C*) at pH 7; (c) 5mg/mL (above C*) at pH 4; (d) 5mg/mL (above C*) at pH 7 as a function of time for three overtones (n=3, 5, and 7; f_0=5MHz) at 24±0.1C.

Figure 18 shows representative QCM-D traces for polymer solutions at concentrations below C* (Figure 18a = pH 4, Figure 18b = pH 7) and above C* (Figure 18c = ph 4, Figure 18d = pH 7). Immediately upon the introduction of polymer solution, the frequency decreased, and the dissipation factor increased for all of the polymer solutions. The extent to which f and D changed and the rate at which the changes occurred were dependent upon polymer concentration and solution pH.

Table 4 provides a summary of measured Δf values for polymer solutions of different concentrations and pH at the equilibrium adsorption stage In general, Δf values are lower for polymer concentrations below C*, and the values increase with increasing concentration. Above C*, however, Δf appears to be constant. For a given polymer concentration, Δf is greater for solutions at pH 4 than for those at pH 7. This is attributed to the changes in the charge states of the HAp substrate and the polymer at different solution pH values. At pH 4, the HAp is expected to be positively charged, while the Gantrez polymer should have a partial negative charge. At pH 7, the HAp is expected to have neutral charge, while the Gantrez polymer should be fully ionized.[53,59,60] Thus, at pH 4 a higher level of ionic interaction is expected between the substrate and the polymer, corresponding to higher levels of adsorbed mass and greater Δf values.

Table 4

Changes in Frequency of the Third Overtone (Δf3) at the Equilibrium Stage of the Polymer Adsorption Process.

Polymer concentration (mg/mL)	Δf3 at pH4 (Hz)	Δf3 at pH 7 (Hz)
0.05	-4.7	-3.0
0.2	-6.3	-4.2
1	-6.7	-5.1
4	-10.3	-9.4
5	-10.4	-9.4

For the solutions with concentration higher than C*, larger changes in dissipation factor and in the separation between overtone curves for ΔD measurements were observed. Large increases in ΔD indicate that the adsorbed layer does not behave as a purely elastic solid, but rather as a viscoelastic material with a significant viscous component. On application of the saline rinse, a sharp reduction in ΔD was observed for the high concentration solutions, with minimal changes in Δf (and thus minimal change in adsorbed mass). This indicates that the viscous layer most likely consisted of a small amount of loosely associated polymer that was removed with the saline rinse, as illustrated in Scheme 4. For the solutions with concentration below C*, only small changes in dissipation factor were observed. It is interesting to note that for the pH 4

solution of low concentration, a decrease in Δf (corresponding to an increase in adsorbed mass) was observed after an injection of the saline rinse solution. This may be attributed to adsorption of salt by the charged G-S97 polymer.

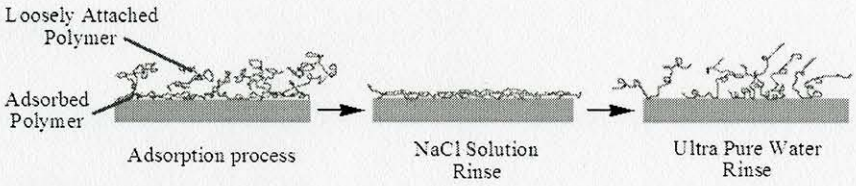

Scheme 4. Polymeric adsorption and desorption processes for polymer layers formed from high concentration (above C*) G-S97solutions: (a) adsorbed polymer was covered by a loosely attached viscous layer; (b) salt solution removed the viscous layer and (c) adsorbed polymer was gradually rinsed off by ultra pure water.

For all solutions, when the DI water rinse was applied a gradual increase in Δf was observed until a stable baseline was reached, indicating removal of the adsorbed polymer layer from the HAp surface. The dissipation factor demonstrated an increase followed by a decrease to a stable baseline, indicating initial formation of a loosely attached viscous layer followed by removal of the polymer from the surface.

The pH of the polymer solution had a large influence on the rate of adsorption and equilibration for the G-S97 solutions. For polymer solutions of pH 4, the saturation plateau was achieved at around 2000 s regardless of the polymer concentration. For solutions of pH 7, on the other hand, equilibrium was not reached even after 4000 s. Many factors have been reported to affect the polymer adsorption process onto a target surface, including polymer structure[61,62] solution conditions[63,41] and polymer-surface interactions.[64] The greater rate of adsorption for the pH 4 solutions is attributed to

electrostatic interactions between the oppositely charged substrate and polymer, as was previously reported by Zhang and coworkers.[27] At pH 7, the polymer-surface interactions are weak due to the reduced ionic interactions, resulting in slower adsorption.

Adsorption kinetics

The adsorption kinetics of polyelectrolytes can be described as a three-step mechanism[65,66]. The first step is the mass transport process, in which polymers diffuse to the proximity of the surface. The second step, the attachment onto the target surface, occurs when polymer chains begin to interact with the surface through secondary interactions including hydrophobic, *van der Waals*, hydrogen bonding, and electrostatic interactions.[67,42,68] The last step is the rearrangement of adsorbed polymers in order to achieve a more stable state. A systematic study of the properties of the adsorbed layer such as initial adsorption rate, adsorbed mass, layer thickness as well as the topography and morphology of the adsorbed layer help provide understanding of the adsorption kinetics.

Adsorption Rate

The strength of the polymer-substrate interaction can be determined from the initial rate of polymer adsorption, if it is assumed that all macromolecules approaching the target surface during this initial stage can be absorbed. To further understand the effect of solution pH and polymer concentration on adsorption behavior, mass increase as a function of time for the first minute of polymer solution flow was determined and is shown in Figure 19.

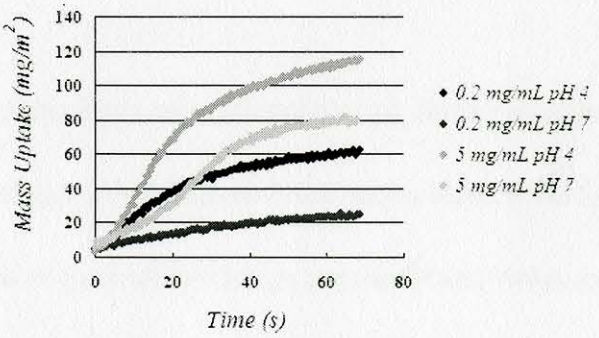

Figure 19. Mass uptake as a function of time for 0.2 and 5 mg/mL G-S97 solutions at pH 4 and 7.

The rate of adsorption, as determined from the initial slope of the curve, is higher for solutions of pH 4, attributed to the stronger electrostatic interactions between the charged G-S97 and HAp surface at low pH. Polymer concentration also affected the initial adsorption rate. At the same pH, higher adsorption rates were observed in more concentrated solutions. For this analysis, the mass uptake was calculated using the Sauerbrey model. The Sauerbrey model assumes a rigid film in the calculation of the adsorbed mass from the measured change in frequency. In this case, the mass change is evaluated only in the first minute of polymer deposition, when it is reasonable to regard the adsorbed polymer layer as a rigid film. Since the adsorbed amount is very small, the polymer is well dispersed, and it can be assumed to homogeneously deposit onto the target surface. Further evidence to support this assumption is the overlapping of Δf traces during the initial stage, which is indicative of a rigid adsorbed layer.[69] Alagha et al.[70] compared the mass of a viscous layer using the Sauerbrey equation with its corrected mass calculated with the Voight model and reported good agreement of the two models at the initial stage of deposition.

D-f Plots

Examination of the frequency and dissipation factors as a D-f plot is a more effective way to investigate adsorption and desorption kinetics than evaluation of the raw QCM-D data, as it shows dissipation change per unit mass, which provides an indication of conformational changes during the process of adsorption.[64,71] If the D-f plot shows a linear relationship, it is assumed that the adsorbed layer maintains a constant conformation during the adsorption process. However, if the relationship is non-linear, this is indicative of a rearrangement of the adsorbed polymer chains. A sharp drop in the D-f plot indicates loss of mass from the adsorbed layer.[72]

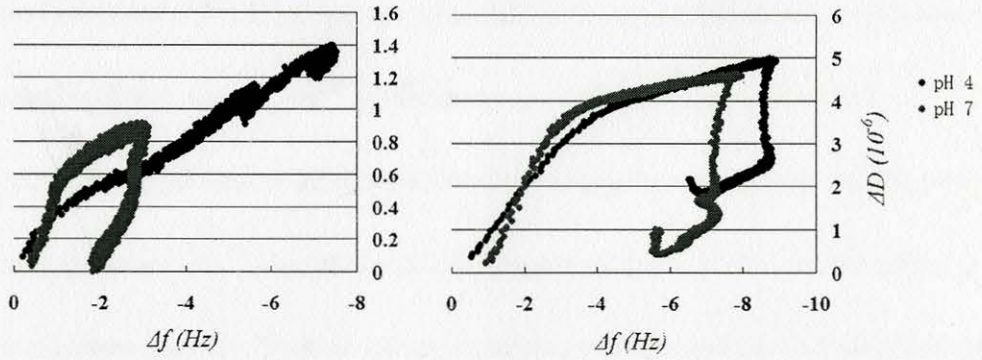

A B

Figure 20. D-f plot for adsorption and desorption of (a) 0.2 mg/mL and (b) 5 mg/mL G-S97 solutions at pH 4 and 7.

Figure 20 displays D-f plots for adsorption (during polymer solution flow) and desorption (during the NaCl solution rinse) of 0.2 (below C*) and 5 mg/mL (above C*) G-S97 solutions at pH 4 and 7. For solutions with concentration below C*, pH has a dramatic effect on the D-f plot. For the pH 4 solution, a linear relationship between *D* and *f* is observed, suggesting that a compact, rigid layer formed on the surface and no

conformational change occurred. For the pH 7 solution, on the other hand, initially a higher slope is observed followed by a change to a lower slope, indicating a transformation of the adsorbed polymer from a viscous to a more rigid layer.[70] After the NaCl rinse solution was applied, a sharp drop in the D-f curve is noted, indicating desorption of the polymer from the surface. The differences in the D-f plots for the two solutions are attributed to the differences in the charge stated for the HAp surface and the polymers in solution at the different pH values. The negatively charged polymer is expected to deposit in a relatively extended state onto the positively charged HAp surface at pH 4. At pH 7, on the other hand, the HAp surface is neutral, attraction of the polymer to the surface is weaker, and polymers adsorb in random conformation with loops and tails extending from the surface.[33] Differences in conformation of adsorbed polyelectrolytes as a function of the nature of the charged surface was also reported by Guzman and coworkers.[66] For solutions of concentration above C*, on the other hand, pH appears to have a smaller effect on adsorption/desorption behavior. D-f plots for the solutions of 5 mg/mL G S-97 demonstrated similar trends at pH 4 and 7 (Figure 20B). They both had much higher ΔD values (over 4×10^{-6}) than those demonstrated for the samples of concentration below C* (less than 1.4×10^{-6}), and both showed discontinuities for Δf values between -7 and -8 Hz. The adsorption/desorption behavior from the solutions above C* is attributed to the development of a viscous layer made up of loosely attached polymer chains, which is primarily driven by polymer-polymer interactions. The large dissipation factor of the loosely attached viscous layer overwhelms the portion due

to the electrostatically bound rigid layer. Thus, differences are observed for the high polymer concentration solutions of different pH only after the removal of the loosely bound layer with the saline rinse.

Morphology Study

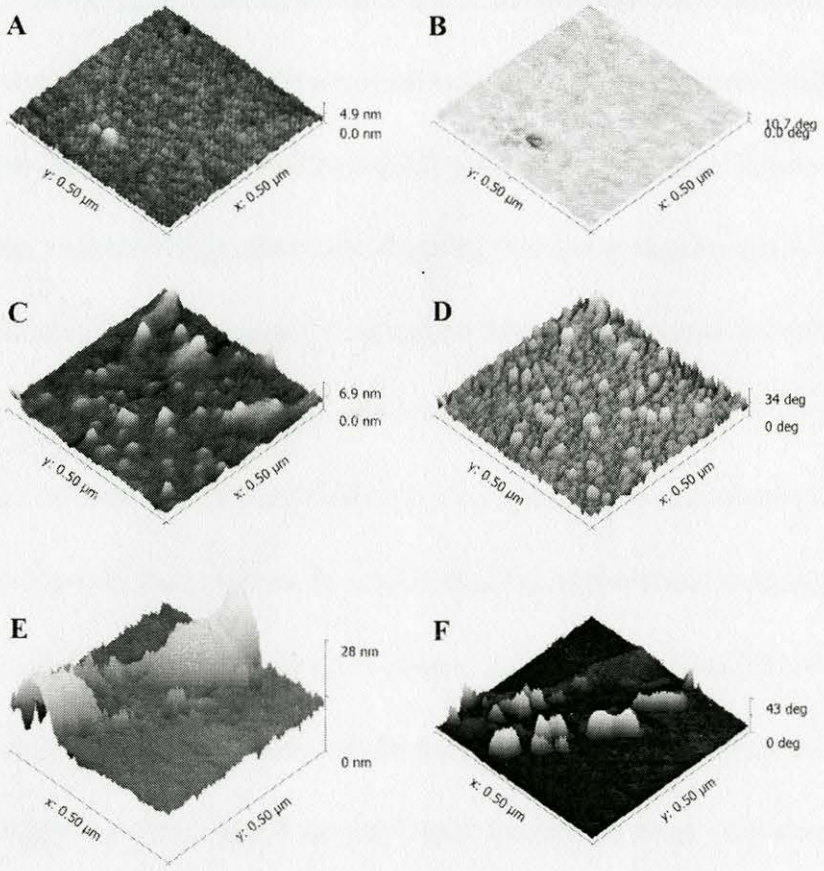

Figure 21. 3D AFM images of pH related adsorption on CaP model surface (left: height, right: phase): (a) and (b) blank CaP model surface; (c) and (d) G-S97adsorption at pH 4; (e) and (f) G-S97 adsorption at pH 7.

AFM height and phase images of the neat CaP surface are shown in Figures 21a and 21b, respectively. The surface is smooth and fairly featureless, with a measured RMS roughness of 0.3 nm. Images of the polymer-coated surfaces obtained from solutions of pH 4 and pH 7 are found in Figures 21cd and 21ef, respectively. The polymer films

adsorbed from the pH 4 solution are continuous and cover the surface with small raised features 10-30 nm in width and measured RMS roughness of 0.7 nm. The homogenous coverage and smooth film surface resulted from the strong electrostatic interactions between the polymer and the surface at pH 4, which allowed strong adsorption and even dispersion of the polymer. The thickness of the adsorbed film was measured to be 2–3 nm by ellipsometry, consistent with the assumed extended charged polyelectrolyte deposition on the surface. The films deposited from pH 7 solutions, on the other hand, appear to be discontinuous and show larger sheet-like deposits that are several hundred nanometers to microns in length. The thickness of this irregular film was measured to be 5-8 nm by ellipsometry, and the RMS roughness measured by AFM was 3.3 nm. The poor coverage on this surface is attributed to the weaker interactions between polymer and substrate at pH 7 and the deposition of polymer in a more random, globular conformation. The observed morphological features in AFM images support the conclusions drawn from QCM-D analysis, in which the adsorbed layers obtained from pH 4 solutions appear to be rigid films, while those obtained from pH 7 solutions appear to be viscoelastic with a viscous, loosely attached outer layer made up of entangled polymer molecules.[33]

Chapter Summary

This study describes quartz crystal microbalance and atomic force microscopy analysis of a poly(methyl vinyl ether-alt-maleic anhydride) copolymer (Gantrez® S97 BF) adsorption on dental mimicking surfaces to determine properties including thickness, morphology, viscoelasticity, and rate of adsorption/desorption of the polymer layer as a

function of the solution environment. A nanoscopically smooth model dental surface was developed for AFM analysis of the adsorbed thin film. It was found that solution pH, salinity, and polymer concentration affected the adsorption process and morphology of the adsorbed polymer layer. A higher rate of adsorption, greater stability, and a more homogeneous deposited film were observed for solutions with pH 4 than for those with pH 7, which was attributed to the charge state of polymer and substrate at the solution pH. Dramatic changes in polymer adsorption and film properties were observed as a function of polymer concentration with respect to the critical overlap concentration.

CHAPTER V

OIL SPILL AND OIL CLEAN-UP

Oil Spill and Its Effect to The Environment

Oil spills occur frequently in the ocean and are regarded as one of the most serious accidents threatening the environment. From the year 2001 to 2010, 900 million tons of crude oil was spilled from different sources which resulted enormous environmental problems all over the world. For example, the Tasman Spirit Greek oil tanker cracked in 2003 causing 28,000 tons of crude oil leakage into the surrounding areas.[73] The Deepwater Horizon oil spill from the British Petroleum (BP) platform occurred on April 20, 2010 and released 210 million gallons of crude oil,[74] one of the largest recorded oil spills ever.

Table 5

10 Largest Oil Spill Accidents in History. Data and Information are from The Telegraph (Reference 74).

Accident	Country/area	Year	Leakage (Mgal.)
Gulf War	Kuwait	1991	240-336
Deepwater Horizon	United States	2010	210
Ixtoc 1 Oil Well	Mexico	1979	140
Atlantic Empress	West Indies	1979	88.3
Fergana Valley	Uzbekistan	1992	87.7
Nowruz Oil Field	Persian Gulf	1983	80
ABT Summer	Off the coast of Angola	1991	80
Castillo de Bellver	South Africa	1983	78.5
Amoco Cadiz	France	1978	68.7
Odyssey Oil Spill	Canada	1988	43

The negative effect of spilled oil on the environment is manifested in several aspects. First, the flowing oil can hinder the photosynthesis of plants and alga in the ocean, reducing food availability and breaking the food chain. Then the toxic components contained in crude oil may release into the water and result in death or harm to marine organisms. Once the spilled oil is washed onto shoreline, it is toxic to plants and animals

inhabiting the coastal marshes. This may result in loss of marshes, which serve as a buffer for storms and wave action for inland cities, resulting in the possibility of further death and destruction.

Oil Spill Remediation Methods

The response for oil spills usually involves containment of oil at the source area followed by recovery and disposal. Mechanical clean-up, chemical clean-up, and natural degradation are common methods employed to remove the spilled oil.[75]

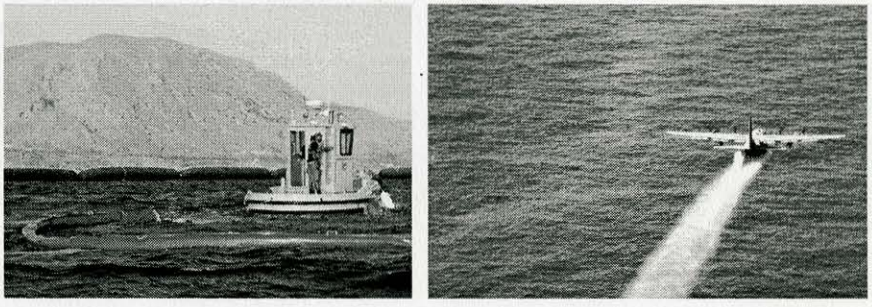

(a) (b)

Figure 22. Illustrations of mechanical and chemical clean-up: (a) A US Navy oil spill response team drills with a "Harbour Buster high-speed oil containment system"; (b) A US Air Force Reserve plane sprays Corexit dispersant over the Deepwater Horizon oil spill in the Gulf of Mexico. Images are from Wikipedia[76]. As works of the U.S. federal government, the images are in the public domain.

In mechanical clean-up, booms are used to contain the crude oil in a specific area, and skimmers are then employed to remove the surface oil and oil-water mixture. During the process, some absorbent materials (usually based on cellulose)[77] are also employed to restrict the mobility of the oil. However, the disadvantage of this method is its high consumption of energy and materials, low efficiency, and great expense.

A number of chemicals are used for chemical clean-up, including dispersants,

gelling agents, burning agents, and sinking agents,[78,79] with dispersants being the most commonly used chemicals. The function of a dispersant is to change the interfacial tension between oil and water and to break the oil into small droplets which can disperse quickly into the water. Although dispersants have high efficiency and relatively low cost, the misuse of dispersing chemicals may result in greater harm to the environment than crude oil itself.[80]

Natural degradation, also known as bioremediation, involves the use of microorganisms capable of degrading oil. There are several prerequisites for the successful deployment of this method. First, natural degradation will not take place directly on the crude oil, so it is necessary to disperse the oil into small particles. As a result, natural degradation usually follows the application of proper dispersants. Moreover, due to the biological activity of bacteria, natural degradation can only be induced in warm environments. Finally, nutrients such as nitrogen and phosphorus are critical for natural degradation. It was found that lack of nutrients might lead to low efficiency of bioremediation.[75]

Oil Dispersant with Anti-Deposition Function

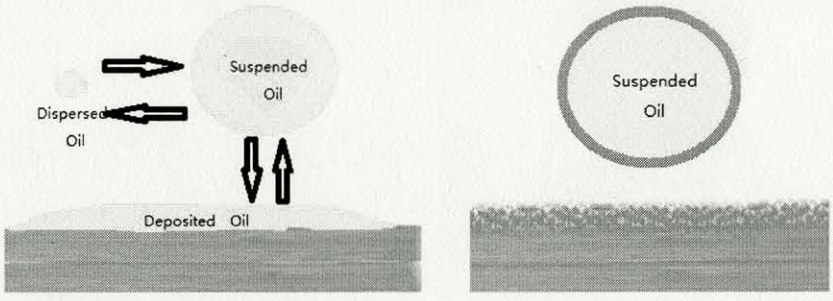

(a) (b)

Figure 23. Comparison of oil dispersant with and without anti-deposition function: (a) without stabilization the dispersed oil still has the chance to aggregate and to deposit; (b) polymeric material can stabilize the oil droplet and prevent the redeposition.

Dispersants are used to break up oil into small droplets and reduce the impact of oil on sea water, shorelines, marine animals, and sea birds. However, the small oil droplets may aggregate and deposit onto land, plant, or animal surfaces. The potential environmental damage from artificial chemicals is also of concern when using dispersants. A safe, nontoxic and environmentally friendly oil dispersant with anti-deposition function is desired.

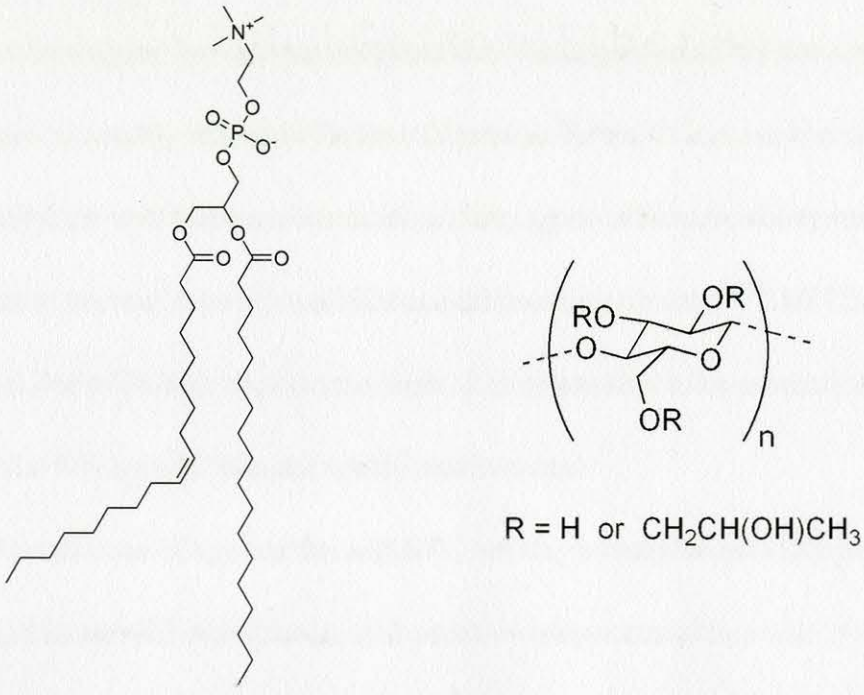

(a) (b)

Figure 24. Structure of (a) soy lecithin and (b) hydroxypropyl cellulose (HPC).

Based on preliminary results obtained in the laboratories of Dr. Robert Lochhead, soy lecithin and hydroxypropyl cellulose (HPC) were selected as the main ingredients to prepare an oil dispersant with anti-deposition function. Soy lecithin is derived from soy beans and is nontoxic. It is an ideal dispersant for such a project: on one hand, it emulsifies the oil into small droplets with large surface area, which is favorable for microbial degradation, and the nitrogen (N) and phosphorus (P) in lecithin will enhance initiation of a bacterial degradation of the oil. On the other hand, lecithin can readily form a lamellar phase, which is an emulsion stabilizing phase. The relative high temperature in the Gulf area and the warm water supplied from the Mississippi River also guarantee the high efficiency of the bacterial degradation of oil. HPC was employed as an

anti-deposition agent that can sterically stabilize the dispersed oil droplets and prevent the aggregation caused by attractive London dispersion forces. It is a member of the cellulose ether family, the well known soil anti-deposition agents which are widely used in laundry detergents to prevent deposition of oils on fabrics during rinsing.[81,82] HPC is safe to organisms due to its high molecular weight. It is impossible to be accumulated in the food chain and is biodegradable in the aquatic environment.

The mixture of soy lecithin and HPC has the potential to provide many advantages in oil spill remediation, as it combines dispersant action and anti-redeposition properties with natural degradation in an environmentally friendly formulation. However, several variables remain to be explored, including the effects of seawater in comparison to fresh water, interaction with sand substrates rather than fabric, and the effects of the dynamic ocean environment on the dispersant performance.

Research Objectives

The goal of this research is to determine the kinetics and adsorption and desorption properties of HPC/soy lecithin oil dispersants on simulated sand surfaces in saline solutions using QCM-D and AFM, while determining the individual function of the formulation ingredients. The objectives of this research are:

1. Evaluate the feasibility of using oxidized Si wafers and SiO_2 coated QCM-D slides as sand mimicking surfaces.

2. Determine the kinetics of adsorption and desorption properties of the HPC/lecithin dispersant using QCM-D on a model sand surface.

3. Determine the morphology of adsorbed films as a function of solution properties and dispersant composition using AFM.

4. Develop an understanding of the structure/property relationships for the dispersant formulations.

CHAPTER VI

OIL DISPERSANT WITH ANTI-DEPOSITION CAPABILITY AND ITS INTERACTION WITH A MODEL SANDSURFACE

Chapter Overview

The mixture of soy lecithin and HPC is a potential oil spill dispersant with anti-deposition function. In this work, atomic force microscopy (AFM) and quartz crystal microbalance with dissipation monitoring (QCM-D) were used to investigate the properties of the selected agents in dry and liquid conditions. SiO_2 coated QCM-D sensors were used as substrates to mimic sand, which is often one of the most difficult substrates to clean once encountered by oil after a spill. Changes in resonance frequency and dissipation for three overtones (n=3, 5 and 7) recorded by QCM-D were fitted with the Voigt viscoelastic model to calculate the thickness of the adsorbed layer. AFM has been used to investigate the morphology of films after deposition on QCM-D slides.

Experimental

Materials

Hydroxypropyl cellulose (HPC, Klucel, type M CS, lot 91470) was purchased from Ashland Inc. Lecithin (Stablec OFM, product code 700553, lot E50361). Detergent-free SAE-30 Shell commercial motor oil was used to simulate spilled oil. All chemicals were used as received.

Solvent

36g/L seawater solution was prepared by dissolving sea salt into 18.2 MΩ cm ultra-pure water, boiling for 15 min for sterilization and filtering through an inorganic membrane filter (pore size: 0.1 μm, Whatman Inc.). The pH value of this seawater was measured to be 8.09 using an Accumet® AR 50 pH meter.

Substrate preparation

Quartz sensor crystals coated with 50nm silicon dioxide (QSX 303, Q-sense, Linthicum Heights, MD) for QCM-D analysis were thoroughly cleaned prior to use. They were first cleaned by UV/ozone treatment for 10 min followed by immersion in a solution of 2% sodium dodecyl sulfate (SDS) in 18.2 MΩ-cm ultra-pure water for 30 min at room temperature. The sensors were then rinsed with 18.2 MΩ-cm ultra-pure water and further cleaned by UV/ozone treatment for 10 min.

Sample Preparation

The samples were prepared by suspending the solutes in simulated sea water with the following compositions: (a) 0.002% (wt.) lecithin in seawater, (b) 0.002% (wt.) HPC in seawater; (c) 0.002% (wt.) oil and 0.002% (wt.) lecithin in seawater, (d) 0.002% (wt.) oil and 0.002% (wt.) HPC in seawater, and (e) 0.002% (wt.) oil, 0.001% (wt.) lecithin and 0.001% (wt.) HPC in sea water. They were first analyzed by QCM, and then the cells were prepared for AFM analysis.

Quartz Crystal Microbalance with Dissipation Monitoring

A QCM-D E4 system (Q-sense) was used at 24±0.1°C. First, a baseline was obtained by flowing saltwater solution through the cell. The baseline was set as the zero point on frequency and dissipation graphs. Once a stable baseline was observed, the samples were injected into the measurement chamber, and changes in frequency and dissipation were recorded as a function of time. Four separate resonant frequencies (overtones, n) were used to drive oscillation of the shear wave through the crystal: (a) 5 MHz (fundamental overtone, n =1), (b) 15 MHz (n =3), (c) 25 MHz (n =5), and (d) 35 MHz (n=7). Since the noise at 5 MHz was very large, we neglected the data on fundamental overtone (n=1) 4. The details of QCM-D technique are described elsewhere.[2]

Atomic Force Microscopy

AFM analysis was performed on the samples after QCM analysis. QCM sensors were quickly dipped in 18.2 MΩ cm ultra-pure water to remove the remnants of salt from the seawater and dried for AFM imaging. The morphology of the samples was investigated using a Dimension 3000 scanning probe microscope in tapping mode. A silicon probe (Veeco, Camarillo, CA) with a nominal force constant of 40 N/m and resonance frequency of 334–390 kHz was used to image samples. AFM imaging was conducted under ambient conditions in a temperature (20°C) and humidity (40-45%) controlled room. Images and statistical quantities were processed with Gwyddion v.2.24 SPM analysis software.

Results and Discussion

Lecithin

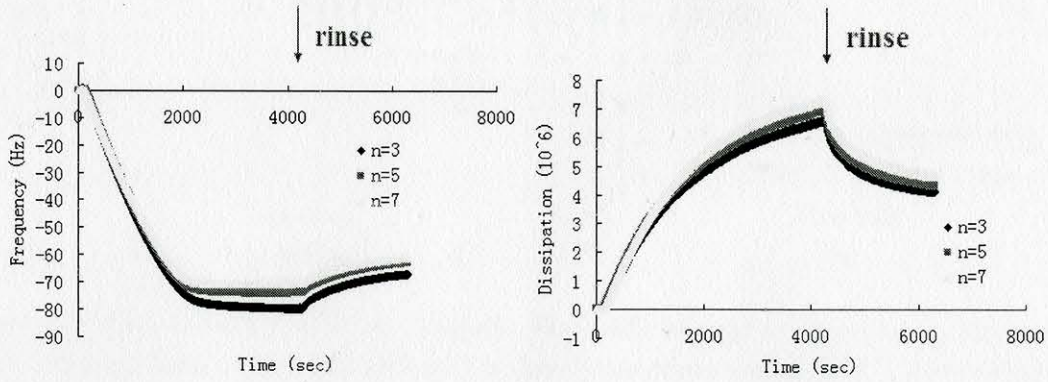

Figure 25. QCM traces of lecithin in seawater. The frequency decreases (a) and the dissipation increases (b) as a function of time (in seconds) for three overtones (n=3, 5, and 7; f_0=5MHz) at 24±0.1 C.

QCM traces for frequency (Figure 25a) and dissipation (Figure 25b) for the lecithin/seawater suspension are shown above. The gradual decrease in frequency and increase in dissipation observed in this system indicate a relatively slow adsorption of lecithin on the silicon dioxide coated sensors. A steady state was achieved after approximately 2000 seconds. The separation of overtones and change in dissipation ratio are evidence for the formation of a viscous layer. The arrow at 4000 seconds indicates an injection of saline solution to rinse the surface. After rinsing for 2000 seconds, the adsorbed lecithin layer was not removed, as indicated by the fact that the frequency and dissipation ratio signals did not return to zero. The thickness of the adsorbed layer is estimated to be 12.6 nm at the completed adsorption and 9.5 nm after rinse.

HPC

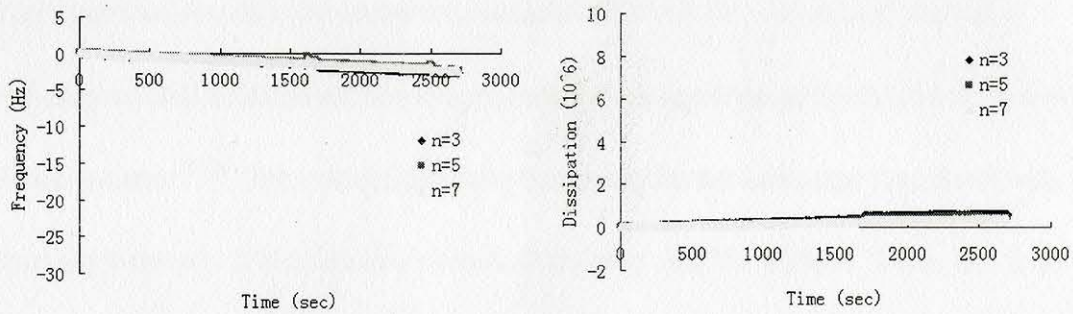

(a) (b)

Figure 26. QCM traces of HPC in seawater. Very little change is observed in frequency (a) or dissipation (b) as a function of time for three overtones (n=3, 5, and 7; f_0=5MHz) at 24±0.1 C.

QCM traces for HPC in seawater are shown in Figure 26. Only minor changes in the frequency and dissipation curves are observed, which are attributed to drift in the instrument over time. No adsorption of the HPC on the silicon dioxide surface was observed.

Oil and lecithin

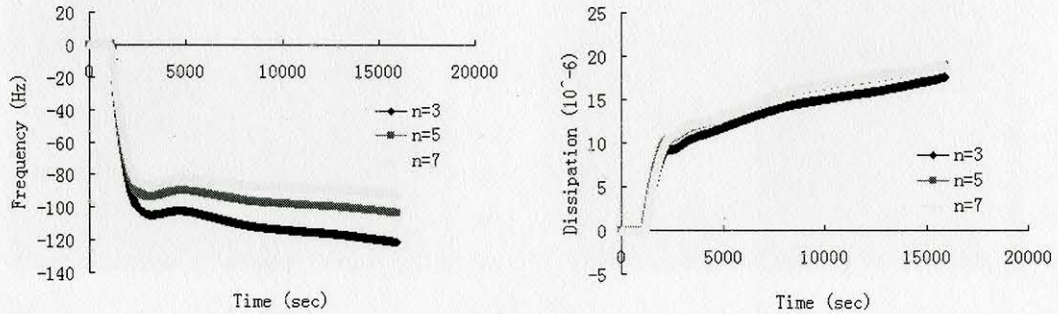

(a) (b)

Figure 27. QCM traces of oil and lecithin in seawater; the frequency decreases (a) and the dissipation increases (b) as a function of time for three overtones (n=3, 5, and 7; f_0=5MHz) at 24±0.1 C.

Figure 27 shows the QCM traces for oil and lecithin in seawater. The frequency decreased and the dissipation increased at a fast rate upon sample injection, which

indicated a fast adsorption process at the initial period. Classic DLVO theory presents an ideal system that accounts for an electric double layer and *Van der Waals* forces in considering colloid attachment, and was reported to be appropriate for dilute oil in water emulsion systems.[83,84] The initial fast adsorption is attributed ionic and *Van der Waals* interactions between the lecithin stabilized oil droplets and the surface. When the SiO2 surface was fully covered, the adsorption rate was reduced, and following that, more droplets were absorbed on the pre-adsorbed layer. The gradual adsorption was not complete until 2.5 h after the sample was injected. The separation of overtones and large change in dissipation ratio are evidence of the formation of a viscoelastic adsorbed layer. The thickness of the adsorbed layer is estimated to be 28 nm at the highest adsorption value (adsorption was not complete at this point) and 23.5 nm after rinse.

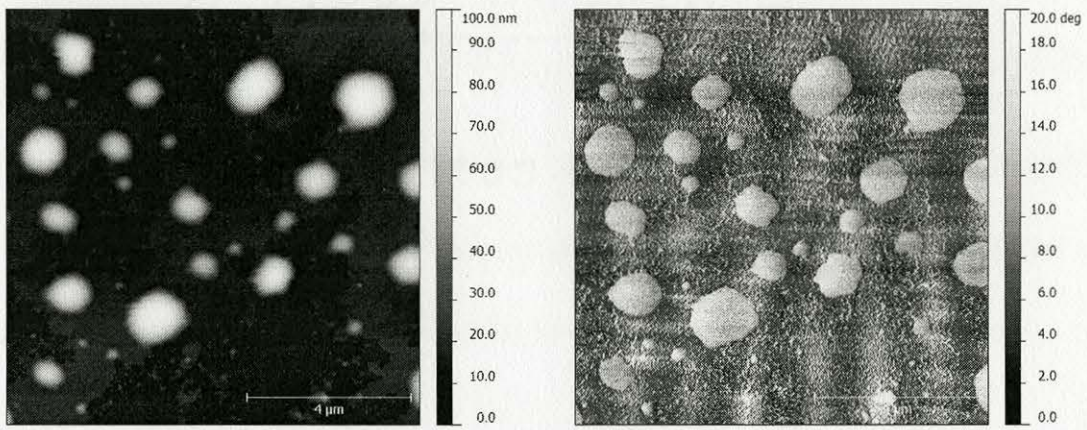

(a) (b)

Figure 28. AFM images of oil and lecithin on the silicon dioxide QCM sensor in height mode (a) and phase mode (b).

Figure 28 shows AFM height (a) and phase (b) images of the QCM sensor for which QCM data is shown above. After QCM analysis, the sensor was briefly dipped in

DI water to remove residual sea salt and dried before AFM imaging. Disc-like particles, ranging in diameter from 250-1540 nm are observed, which are attributed to emulsified oil droplets adsorbed to the surface. The AFM images combined with the QCM analysis indicate that lecithin disperses the floating oil in seawater but does not prevent deposition on the silicon dioxide surface.

Oil and HPC

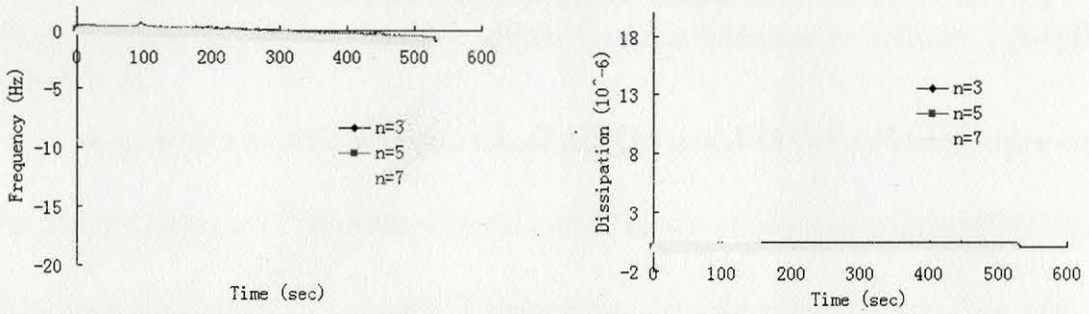

(a) (b)

Figure 29. QCM traces of oil and HPC in seawater. There is no obvious change in frequency (a) or dissipation (b) as a function of time for three overtones (n=3, 5, and 7; f_0=5MHz) at 24±0.1 C.

QCM traces for HPC in seawater are shown in Figure 29. Only minor changes in the frequency and dissipation curves are observed, which are attributed to drift in the instrument over time. No adsorption of the HPC on the silicon dioxide surface was observed.

Oil, Lecithin, and HPC

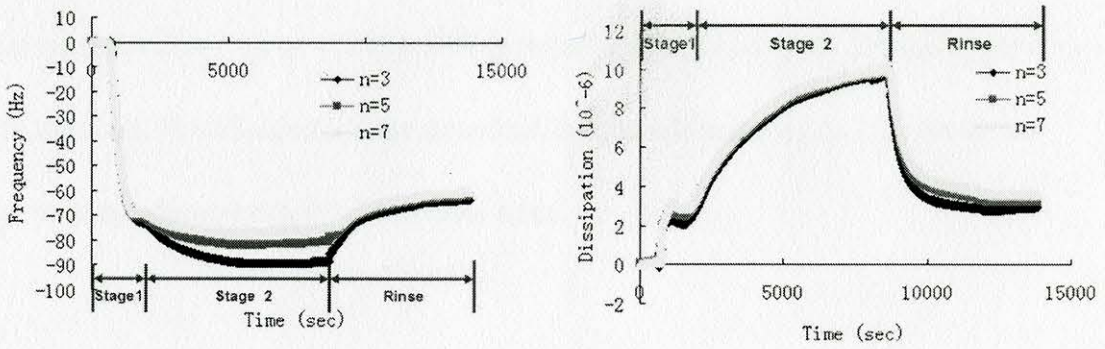

(a) (b)

Figure 30. Adsorption of oil lecithin and HPC, the frequency decreases (a) and the dissipation increases (b) as a function of time for three overtones (n=3, 5, and 7; f_0=5MHz) at 24±0.1 C.

Figure 30 shows QCM traces for oil, lecithin, and HPC dispersions in seawater. For these samples, two adsorption stages were observed. Upon the injection of the sample, frequency decreased and dissipation increased sharply, and a short-lived plateau was observed (stage 1). In stage 2, the frequency decreases at a slow rate, and dissipation increases at a slow rate. The rapid change in frequency and dissipation is a sign of fast adsorption, which is attributed to the interaction of substrate and oil droplets as discussed earlier. In stage 2, the adsorption curve is similar to that of lecithin. A reasonable explanation is the adsorption of oil droplets was saturated, but the adsorption of lecithin was not complete. Moreover, if comparing the changes of frequency and dissipation ratio on the third overtone, the values were found to be much higher for the mixture than pure lecithin. The difference is due to the contribution of the adsorbed oil droplets. In the third stage, after the surface was rinsed by seawater, the great increase in frequency and decrease in dissipation ratio indicated a large amount of mass was lost in this process.

The final values of frequency and dissipation ratio are similar to that of a pure lecithin sample after rinse. Thus, we may assume most of the adsorbed oil droplets were removed by the rinse. The thickness of the adsorbed layer is estimated to be 15.5 nm at the completed adsorption and 8.0 nm after rinse.

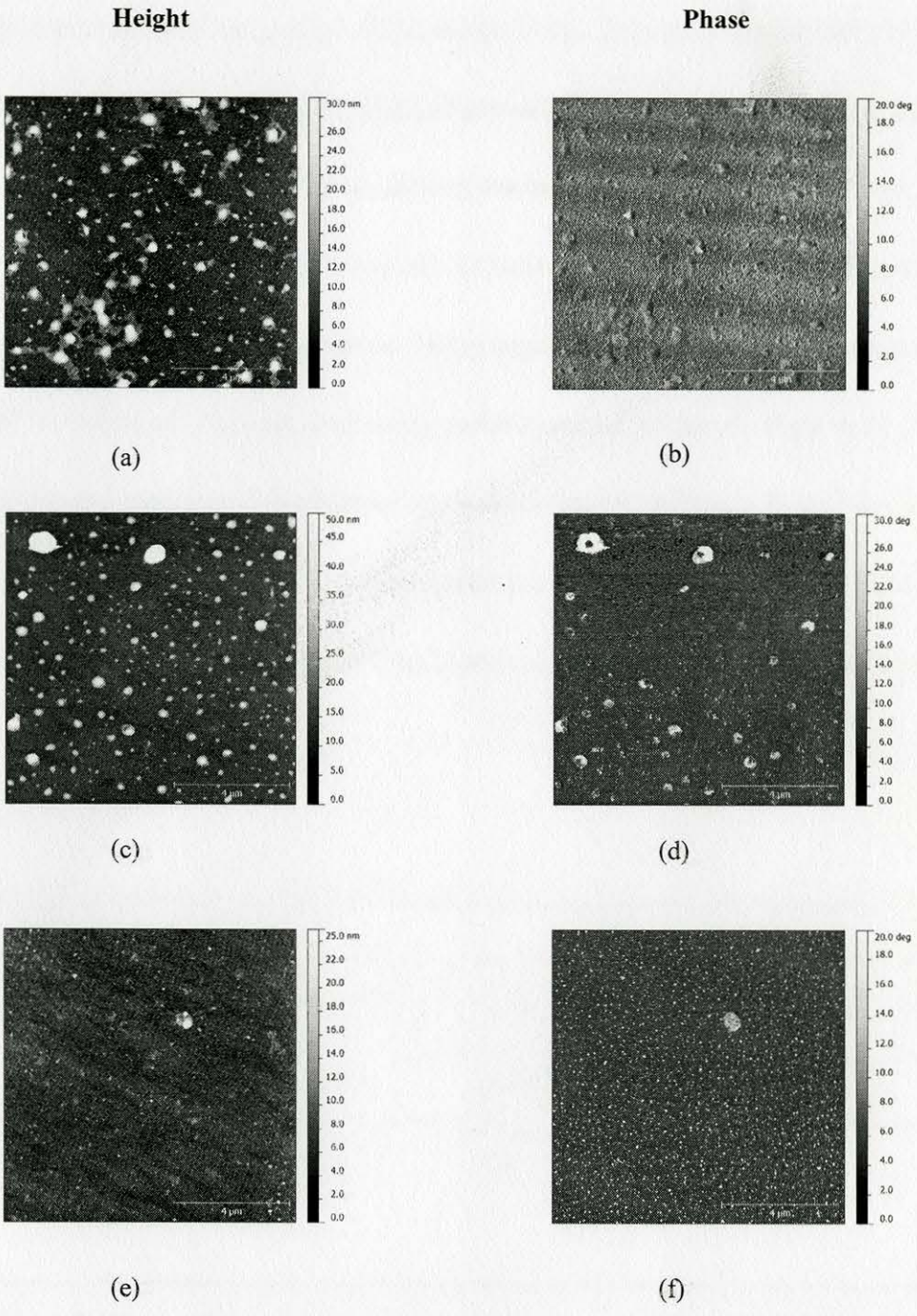

Figure 31. AFM height and phase images of oil lecithin and HPC spread on the silicon dioxide QCM sensors at stage 1(a and b), stage 2(c and d), and after rinse by seawater (e and f).

For the sample of oil lecithin and HPC, three parallel QCM-D measurements were operated to ensure the synchronization and accuracy. The morphology of sensors at stage

1, 2, and after rinse was imaged by AFM, respectively. Figures 31 (a) and (b) are height and phase images at stage 1. In this stage, dispersed oil droplets were adsorbed onto the substrate quickly. Compared with the oil droplets emulsified only by lecithin, the mixture of lecithin and HPC reduced the size of oil droplets dramatically. Figures 31 (c) and (d) are images at stage 2, which show more highly separated droplets and evidence of "hollow" or collapsed particles, indicating partial removal of the oil. Figures 31 (e) and (f) are height and phase images corresponding to the sensor after rinse. Most of the adsorbed droplets were removed, which is consistent with the QCM-D result. Both the AFM and QCM-D results indicated that the HPC/lecithin mixture prevented the droplets from being deposited.

Table 6

Thickness of Adsorbed Layers and Dimensions of Absorbed Oil Droplets. (unit: nm)

	Thickness of layer (before rinse)	Thickness of layer (after rinse)	Diameter of oil droplets
Lecithin	12.6	9.5	None
Lecithin and oil	28(not a completed adsorption)	23.5	250-1540
Lecithin, HPC and oil	15.5	8.0	60-420

The estimated thickness of adsorbed layers for lecithin, and the mixture of lecithin, HPC, and oil are similar, which indicate the adsorbed layers mainly consisted of lecithin. But for the mixture of lecithin and oil, the thickness value was much higher than the others. One may conclude the increased thickness was the contribution of a large amount of adsorbed oil. On incorporation of HPC, the adsorbed layer is much smaller, and the diameter of the oil droplets is smaller. Thus, the HPC/lecithin mixture provides dispersible oil droplets which are not re-adsorbed on the surface.

Chapter Summary

QCM-D and AFM were used to understand the adsorption properties and morphology of different formulations of the oil spill dispersant. Lecithin, as a dispersant, emulsifies the floating oil to form a droplet, but does not prevent redeposition on the simulated sand surface. HPC does not disperse the floating oil. The mixture of lecithin and HPC is an ideal detergent, which disperses the floating oil into very small droplets and prevents the reddeposition of oil. The small suspended oil droplet is an ideal structure for biological degradation of the oil.

CHAPTER VII

CONCLUSIONS

This thesis involved two projects. The first was a study of the adsorption of G-S97 on dental mimicking surfaces, which employed QCM-D, AFM, and ellipsometry analysis. HAp coated QCM-D slides were used as dental mimicking surfaces for QCM-D studies. Three methods were attempted to produce a nanoscopically smooth model dental surface for morphology studies of adsorbed polymer thin films. AFM and SEM results indicated that the substrates developed from nucleation and phosphorylation methods provided films with low roughness (< 5nm). However, the nucleated CaP layer showed very poor stability on exposure to DI water. The CaP coated surface developed using the phosphorylation method was selected as the model substrate for this work because it provided a smooth (RMS roughness ~0.3 nm), stable film with composition similar to that of the natural tooth surface. The studies showed that the adsorption mechanisms and kinetics of Gantrez® S-97 were impacted by the pH of the deposition solution, attributed to differences in the charged state of the HAp surface and to the concentration of the polymer in solution. At pH 4, the HAp substrate was positively charged, resulting in strong electrostatic interactions between the partially negatively charged polyelectrolyte and the surface. Under these conditions and with low polymer solution concentration, the adsorption rate was relatively high, and a flat, compact rigid polymer layer, was formed that homogeneously covered the model surface. No conformational changes were observed during deposition of this layer and the desorption of the polymer during the

NaCl solution rinse was negligible. At pH 7 the charge density of the HAp surface was sharply reduced, resulting in lower levels of electrostatic interaction of the negatively charged polymer molecules with the surface. The polymer adsorbed onto the surface with loop and tail structures, and films were inhomegeneous due to weak polymer-surface interactions. High measured dissipation factor for films deposited under these conditions suggested the formation of a loosely attached polymer layer entangled with the loop and tail structures, which was removed by a saline rinse. Adsorption was found to be proportional to polymer concentration for dilute solutions, but it reached saturation at or above C*. A viscous layer formed by loosely attached polymer chains was observed in all solutions of concentration greater than C*, attributed to polymer-polymer interactions in concentrated solution. The adsorbed polymer was gradually removed from the polymer during an ultra pure water rinse, indicating that a certain level of ionic strength is necessary to maintain adsorption on the dental surface. The results of these findings provide information on the kinetics of adsorption, morphology of adsorbed layers, and desorption processes of pH responsive polymers in contact with pH responsive dental-mimicking surfaces. Theses findings should prove useful in defining avenues for advancement of new polymer systems and formulations for oral care applications.

The goal of the second project was to evaluate the performance of a biopolymer-based oil dispersant with anti-deposition function. The main ingredients of the oil cleaner are soy lecithin and HPC, which are the dispersant and the oil anti-deposition agent, respectively. In this research the function of each ingredient in the

formulation, as well as the comprehensive performance of the oil spill cleaner, were tested in sea water. QCM-D and AFM were used to understand the adsorption properties and morphology of oil in the presence of different formulations. Lecithin, as a dispersant, emulsified the floating oil to form droplets but did not prevent the redeposition of oil on a model sand surface. HPC did not disperse the floating oil. The mixture of lecithin and HPC is an ideal oil spill cleaner, which dispersed the floating oil into very small droplets and prevented the redeposition of oil. The small suspended oil droplet is an ideal structure for biological degradation of the oil.

CHAPTER VIII

RECOMMENDATIONS FOR FUTURE RESEARCH

The experiments and discussion in this thesis have successfully developed an understanding of the solution factors, especially pH and polymer concentration on the adsorption kinetics of G-S97. However, some additional fundamental questions considering the effects of other solution factors, polymer structure, as well as the substrate properties are recommended for future research.

How do other solution factors affect the polymeric adsorption on dental surface?

This research mainly focused on the effect of pH values and solution concentrations on the polymeric adsorption on dental surface. The effect of salt ion types and concentration has not been studied. It is predicted that the screening effect from free ions may result in different strengths of polymer-surface interactions, which are expected to lead to differences in adsorption behaviors. Future research conducting polymer adsorption studies in different salt solutions is recommended.

How does the polymer structure affect the polymeric adsorption on dental surfaces?

To understand the effect of polymer structure on adsorption to dental surface, two studies are recommended. The first is an evaluation of the effect of changes in the polymer molecular weight. Changes in molecular weight may result in different diffusion rates when the polymer approaches the target surface. A comprehensive study of adsorption kinetics and adsorbed morphology of polymers with different molecular

weight may help to provide a greater fundamental understanding of the adsorption mechanism. The second recommended study involves the effect of side groups on the polymer chain. Changing the hydrophobicity of the side group may influence the polymeric conformation in the solution and may also result in variation in polymer-surface interactions. Gantrez® polymers could be modified with different side groups and be used as model polymers for future research.

Other factors, such as the roughness of the target surface may also influence the adsorption behavior. Generally, improving the fundamental understanding of these factors would be helpful to guide the development and formulation of polymers in personal care products.

REFERENCES

(1) Magonov, S. N. In *Encyclopedia of Analytical Chemistry*; John Wiley & Sons, Ltd: 2006.

(2) Sauerbrey, G. *Zeitschrift für Physik A Hadrons and Nuclei* **1959**, *155*, 206.

(3) Lüthgens, E.; Herrig, A.; Kastl, K.; Steinem, C.; Reiss, B.; Wegener, J.; Pignataro, B.; Janshoff, A. *Meas. Sci. Technol.* **2003**, *14*.

(4) Höök, F.; Rodahl, M.; Brzezinski, P.; Kasemo, B. *Langmuir* **1998**, *14*, 729.

(5) Feldoto, Z.; Pettersson, T.; Dėdinaitė, A. *Langmuir* **2008**, *24*, 3348.

(6) Fujimoto, J.; Petri, D. F. S. *Langmuir* **2000**, *17*, 56.

(7) Kockisch, S.; Rees, G. D.; Young, S. A.; Tsibouklis, J.; Smart, J. D. *J. Pharm. Sci.* **2003**, *92*, 1614.

(8) International Specialty Products Company: 2003.

(9) Kon'kov, A. S.; Pustovalova, O. L.; Agapov, I. I. *Appl. Biochem. Microbiol.* **2010**, *46*, 739.

(10) Irache, J.; Huici, M.; Konecny, M.; Espuelas, S.; Campanero, M.; Arbos, P. *Molecules* **2005**, *10*, 126.

(11) Wang, L. J.; Tang, R.; Bonstein, T.; Bush, P.; Nancollas, G. H. *Journal of Dental Research* **2006**, *85*, 359.

(12) Hu, Y.; Smith, G. L.; Richardson, M. F.; McCormick, C. L. *Macromolecules* **1997**, *30*, 3526.

(13) Hu, Y.; Armentrout, R. S.; McCormick, C. L. *Macromolecules* **1997**, *30*, 3538.

(14) Jeong, J.-H.; Byoun, Y.-S.; Lee, Y.-S. *React. Funct. Polym.* **2002**, *50*, 257.

(15) Fang, W.; Cai, Y.; Chen, X.; Su, R.; Chen, T.; Xia, N.; Li, L.; Yang, Q.; Han, J.; Han, S. *Bioorganic & Medicinal Chemistry Letters* **2009**, *19*, 1903.

(16) Popa, M.; Sunel, V.; Dulea, N.; Popa, A. A.; Ottenbrite, R. M.; Uglea, C. V. *J. Bioact. Compat. Polym.* **2007**, *22*, 651.

(17) Osaki, T.; Werner, C. *Langmuir* **2003**, *19*, 5787.

(18) Yoshida, Y.; Meerbeek, B.; Nakayama, Y.; Snauwaert, J.; Hellemans, L.; Lambrechts, P.; Vanherle, G.; K. Wakasa *Journal of Dental Research* **2000**, *79*, 709.

(19) Borja; Michael, J. In *Pat. Appl. Publ.*; office, U. p. t., Ed. US, 2011; Vol. A1 20110317.

(20) Woolfson, A. D.; McCafferty, D. F.; McCallion, C. R.; McAdams, E. T.; Anderson, J. M. *J. Appl. Polym. Sci.* **1995**, *56*, 1151.

(21) Irina Popesscu; Dana Mihalea Suflet; Irina Mihaela Peline; Chitanyu, G. C. *Revue Roumaine de Chimie* **2010**, *56*, 173.

(22) http://www.innovadex.com

(23) Wilson, A. D.; Prosser, H. J.; Powis, D. M. *Journal of Dental Research* **1983**, *62*, 590.

(24) Yoshida, Y.; Meerbeek, B. V.; Nakayama, Y.; Yoshioka, M.; Snauwaert, J.; Abe, Y.; Lambrechts, P.; Vanherle, G. *Journal of Dental Research* **2001**, *80*, 1565.

(25) Staines, M.; Robinson, W. H.; Hood, J. A. A. *J. Mater. Sci.* **1981**, *16*, 2551.

(26) Ravaglioli, A.; Krajewski, A. *Bioceramics: Materials, properties, applications*; Chapman & Hall (London and New York), 1992.

(27) Wei, M.; Ruys, A. J.; Milthorpe, B. K.; Sorrell, C. C.; Evans, J. H. *Journal of Sol-Gel Science and Technology* **2001**, *21*, 39.

(28) McGall, S. J.; Davies, P. B.; Neivandt, D. J. *The J. Phys. Chem. A* **2005**, *109*, 8745.

(29) Toworfe, G. K.; Composto, R. J.; Shapiro, I. M.; Ducheyne, P. *Biomaterials* **2006**, *27*, 631.

(30) Kim, S. M.; Ahn, S. J.; Lee, H.; Kim, E. R.; Lee, H. *Ultramicroscopy* **2002**, *91*, 165.

(31) Long, M. H., The Institute of Paper Science and Technology, 1994.

(32) M. Elimelech; J. Gregory; X. Jia; Williams, R. A. *Particle Deposition and Aggregation - Measurement, Modelling and Simulation*; Elsevier: Boston, 1995.

(33) Morgan, S. E.; Jones, P.; Lamont, A. S.; Heidenreich, A.; McCormick, C. L. *Langmuir* **2006**, *23*, 230.

(34) Song, X.; Cao, M.; Han, Y.; Wang, Y.; Kwak, J. C. T. *Langmuir* **2007**, *23*, 4279.

(35) Belton, D.; Stupp, S. I. *Macromolecules* **1983**, *16*, 1143.

(36) Briones, X. G.; Encinas, M. V.; Petri, D. F. S.; Pavez, J. E.; Tapia, R. A.; Yazdani-Pedram, M.; Urzúa, M. D. *Langmuir* **2011**.

(37) Urzúa, M. D.; Briones, X. G.; Carrasco, L. P.; Encinas, M. V.; Petri, D. F. S. *Polymer* **2010**, *51*, 3445.

(38) D.F, S.; P.W, A. *Inorganic Chemistry* 3rd ed.; Oxford University: Oxford, 1999; Vol. 5.

(39) Begala, A. J.; Strauss, U. P. *The J. Phys. Chem.* **1972**, *76*, 254.

(40) Pagac, E. S.; Prieve, D. C.; Tilton, R. D. *Langmuir* **1998**, *14*, 2333.

(41) Zhang, X.; Sun, Y.; Gao, M.; Kong, X.; Shen, J. *Macro. Chem. Phys.* **1996**, *197*, 509.

(42) Van de Steeg, H. G. M.; Cohen Stuart, M. A.; De Keizer, A.; Bijsterbosch, B. H. *Langmuir* **1992**, *8*, 2538.

(43) Guzmán, E.; Ortega, F.; Baghdadli, N.; Luengo, G. S.; Rubio, R. G. *Colloids and Surf. A: Physicochemical and Engineering Aspects* **2011**, *375*, 209.

(44) Strauss, U. P.; Barbieri, B. W.; Wong, G. *The J. Phys. Chem.* **1979**, *83*, 2840.

(45) Sugai, S.; Nitta, K.; Ohno, N. *Polymer* **1982**, *23*, 238.

(46) Sugai, S.; Ohno, N.; Nitta, K. *Macromolecules* **1974**, *7*, 961.

(47) Ohno, N.; Nitta, K.; Makino, S.; Sugai, S. *Journal of Polymer Science: Polymer Physics Edition* **1973**, *11*, 413.

(48) Ohno, N.; Okuda, T.; Nitta, K.; Sugai, S. *Journal of Polymer Science: Polymer Physics Edition* **1978**, *16*, 513.

(49) Martin, P. J.; Morss, L. R.; Strauss, U. P. *J. Phys. Chem.* **1980**, *84*, 577.

(50) Barbieri, B. W.; Strauss, U. P. *Macromolecules* **1985**, *18*, 411.

(51) Dubin, P.; Strauss, U. P. *The J. Phys. Chem.* **1973**, *77*, 1427.

(52) Olea, A. F.; Barraza, R. G.; Fuentes, I.; Acevedo, B.; Martinez, F. *Macromolecules* **2001**, *35*, 1049.

(53) *Gantrez® Copolymers Technical Profile*; International Specialty Products Inc (ISP®), 1999.

(54) Wei, Y., The University of Southern Mississippi, 2012.

(55) Irwin, E. F.; Ho, J. E.; Kane, S. R.; Healy, K. E. *Langmuir* **2005**, *21*, 5529.

(56) Dutta, A. K.; Belfort, G. *Langmuir* **2007**, *23*, 3088.

(57) Sahagun, C. M.; Morgan, S. E. *ACS Applied Materials & Interfaces* **2012**, *4*, 564.

(58) Linow, K. J. *Acta Polymerica* **1983**, *34*, 447.

(59) Zhang, J.; Maeda, M.; Kotobuki, N.; Hirose, M.; Ohgushi, H.; Jiang, D.; Iwasa, M. *Mater. Chem. and Phys.* **2006**, *99*, 398.

(60) Mafé, S.; Garcia-Morales V, Ramirez P. *Chem. Phys.* **2004**, *296*, 29.

(61) Tsuchida, A.; Matsuura, K.; Kobayashi, K. *Macromol. Chem. and Phys.* **2000**, *201*, 2245.

(62) Ondaral, S.; Wågberg, L.; Enarsson, L.-E. *J. Colloid Interface Sci.* **2006**, *301*, 32.

(63) Saarinen, T.; Österberg, M.; Laine, J. *Colloids Surf. A* **2008**, *330*, 134.

(64) Sedeva, I. G.; Fornasiero, D.; Ralston, J.; Beattie, D. A. *Langmuir* **2009**, *25*, 4514.

(65) Gregory, J. *Polym. Int.* **1995**, *36*, 102.

(66) Guzmán, E.; Ortega, F.; Baghdadli, N.; Cazeneuve, C.; Luengo, G. S.; Rubio, R. n. G. *ACS Applied Materials & Interfaces* **2011**, *3*, 3181.

(67) Silva, R. A.; Urzúa, M. D.; Petri, D. F. S. *J. Colloid Interface Sci.* **2009**, *330*, 310.

(68) Rojas, O. J.; Ernstsson, M.; Neuman, R. D.; Claesson, P. M. *Langmuir* **2002**, *18*, 1604.

(69) Steinem, C.; Janshoff, A. *Piezoelectric sensors*; Springer, **2007**; Vol. 5.

(70) Alagha, L.; Wang, S.; Xu, Z.; Masliyah, J. *The Journal of Physical Chemistry C* **2011**, *115*, 15390.

(71) Slavin, S.; Soeriyadi, A. H.; Voorhaar, L.; Whittaker, M. R.; Becer, C. R.; Boyer, C.; Davis, T. P.; Haddleton, D. M. *Soft Matter* **2012**, *8*, 118.

(72) Sedeva, I. G.; Fetzer, R.; Fornasiero, D.; Ralston, J.; Beattie, D. A. *J.Colloid and Interface Sci.* **2010**, *345*, 417.

(73) Diemand, R.; Francis, K., Worcester Polytechnic Institute, 2011.

(74) http://www.telegraph.co.uk/news/worldnews/australiaandthepacific/newzealand/8812598/10-largest-oil-spills-in-history.html

(75) *Bioremediation for Marine Oil SpillsSpills—Background Paper*; Westermeyer, W. E., Ed.; Government Printing Office: Washington DC, U.S., 1991.

(76) http://en.wikipedia.org/wiki/Oil_spill

(77) Teas, C.; Kalligeros, S.; Zanikos, F.; Stournas, S.; Lois, E.; Anastopoulos, G.

Desalination **2001**, *140*, 259.

(78) Hanabusa, K.; Matsumoto, Y.; Miki, T.; Koyama, T.; Shirai, H. *Journal of the Chemical Society, Chemical Communications* **1994**, *0*, 1401.

(79) Freiberger, A.; Byers, J. M. *International Oil Spill Conference Proceedings* **1971**, *1971*, 245.

(80) Nelson-Smith, A. In *Chemical Dispersants for the Control of Oil Spills: A Symposium*; ASTM International: 1978; Vol. 659, p 253.

(81) Ruppert, R. M.; Savio, L. E.; Google Patents: 1986.

(82) Secemski, I. I.; Lander, L. H.; Princen, H. M.; Google Patents: 1986.

(83) Soma, J.; Papadopoulos, K. D. *Colloids Surf. A* **1995**, *101*, 51.

(84) Malmsten, M.; Lindström, A.-L.; Wärnheim, T. *J. Colloid Interface Sci.* **1996**, *179*, 537.